2.14 Properties of Rocks and Minerals – Constitutive Equations, Rheological Behavior, and Viscosity of Rocks

D. L. Kohlstedt, University of Minnesota, Minneapolis, MN, USA

2.14.1 Introduction

The rheological behavior of mantle rocks determines the mechanical response of lithospheric plates as well as the nature of convective flow in the deeper mantle. Geodynamic models of these large-scale processes require constitutive equations that describe rheological properties of the appropriate mantle rocks. The forms of such constitutive equations (flow laws or combinations of flow laws) are motivated by micromechanical analyses of plastic deformation phenomena based on physical processes such as ionic diffusion, dislocation migration, and grain-boundary sliding. Critical parameters in flow laws appropriate for rock deformation such as the dependence of strain rate on stress, grain size, temperature dependence (activation energy), and pressure dependence (activation volume) must be determined from careful, well-designed laboratory experiments. Geophysical observations of the mechanical behavior of Earth's mantle in response to changes in the stress environment due for example to an earthquake or the retreat of a glacier provide tests of the applicability of the resulting constitutive equations to deformation occurring under geological conditions.

Confident extrapolation of flow laws determined under laboratory conditions requires an understanding of the physical processes involved in deformation. Minerals and rocks deform plastically by a number of different mechanisms, each of which requires defects in the crystalline structure. Diffusion creep involves the movement of atoms or ions and thus of point defects; dislocation creep entails the glide and climb of line defects; grain-boundary sliding necessitates motion along planar defects. Within any deformation regime, more than one deformation process may be important. For example, diffusion creep can be divided into a regime dominated by diffusion along grain boundaries and another dominated by diffusion through grain interiors (the so-called grain matrix). Grain size, temperature, and pressure dictate which of these two processes is more important. Likewise, in dislocation creep, deformation can be divided into low-temperature and high-temperature regimes, with glide controlling the rate of deformation in the

former and climb in the latter. As temperature decreases, differential stress necessarily increases if deformation is to continue at a given rate.

Plastic deformation is a thermally activated, kinetic, irreversible process. Experimentalists frame laboratory investigations of plastic deformation in terms of strain rate as a function of differential stress, temperature, pressure, grain size, and other thermomechanical and structural parameters. In contrast, geodynamicists cast plasticity in terms of viscosity, the ratio of stress to strain rate. In both cases, flow laws or constitutive equations describe the relationships between these parameters, thus providing the basis for extrapolating from laboratory to Earth conditions. Tests of the appropriateness of laboratory-derived flow laws to processes occurring in Earth at much slower strain rates (higher viscosities) – and thus necessarily much lower stresses and/or much lower temperatures and/or much coarser grain sizes – include comparisons of microstructures observed in experimentally deformed samples with those in naturally deformed rocks and of viscosities derived from laboratory experiments with those determined from geophysical observations.

The present chapter, therefore, starts with an examination of the role of defects in plastic deformation, including a discussion of the influence of water-derived point defects on kinetic processes. Next, a section on some of the important mechanisms of deformation introduces constitutive equations that describe plastic flow by linking thermomechanical parameters such as strain rate, differential stress, temperature, pressure, and water fugacity with structural parameters such as dislocation density, grain size, and melt fraction. Finally, profiles of viscosity versus depth in the upper mantle are used to test the applicability of flow laws determined from micromechanical models and laboratory experiments to plastic flow taking place deep beneath Earth's surface.

2.14.2 Role of Lattice Defects in Deformation

Defects in rocks are essential for plastic deformation to proceed. Zero-dimensional or point defects (specifically vacancies and interstitials) allow flow by diffusive transport of ions, one-dimensional (1-D) or line defects (dislocations) permit deformation by glide and climb, and 2-D or planar defect (grain–grain interfaces) facilitate deformation by grain-boundary sliding and migration. More than one type of defect may be simultaneously involved in deformation. For example, diffusion creep involves not only diffusion but also grain-boundary sliding (Raj and Ashby, 1971), dislocation processes also frequently couple with grain-boundary sliding (Langdon, 1994), and dislocation creep necessitates glide on several slip systems often combined with climb (von Mises, 1928; Groves and Kelly, 1969; Kelly and Groves, 1969; Paterson, 1969). In addition, dynamic recrystallization frequently acts as a recovery mechanism, producing a new generation of dislocation-free grains that are more easily deformed than the parent grains (e.g., Tullis and Yund, 1985; de Bresser *et al.*, 2001; Drury, 2005). In this section, some fundamental aspects of point defects, dislocations, and grain boundaries are introduced as background for discussing the rheological behavior of rocks and the associated constitutive equations.

2.14.2.1 Point Defects – Thermodynamics and Kinetics

2.14.2.1.1 Thermodynamics

At temperatures above absolute zero, in thermodynamic equilibrium crystalline grains contain finite populations of vacancies and self-interstitials. Although the enthalpy of a crystal increases linearly with the addition of vacancies or self-interstitials, the entropy decreases nonlinearly. Hence, the Gibbs free energy of a crystal is minimized not when the crystal is perfect (i.e., defect free) but rather when the crystal contains a finite concentration of vacancies and self-interstitials (i.e., when the crystal is imperfect) (see e.g., Devereux, 1983, pp. 296–300). In metals, the concentrations of these point defects in thermodynamic equilibrium are determined by temperature and pressure through their Gibbs energies of formation (Schmalzried, 1981, pp. 37–38). In ionic materials, the situation is more complicated because the concentrations of the different types of point defects are coupled through the necessity for electroneutrality, which requires that the sum of the concentrations of the various types of positively charged point defects equals the sum of the concentrations of all of the negatively charged point defects (Schmalzried, 1981, pp. 38–42). The concentration of one type of positively charged point defect often greatly exceeds the concentrations of the other positively charged point defects; a similar situation will exist for negatively charged defects. This combination of positive and negative defects defines the majority point defects or the defect type. The charge neutrality condition is then approximated by

equating the concentration of the positively charged to the concentration of the negatively charged majority point defects. An example serves to illustrate the salient elements of point defect thermodynamics.

Consider the case of a simple metal oxide, MeO, where Me is an ion such as Mg, Ni, Co, Mn, or Fe. Structural elements for this system include $Me^{\times}_{Me}$, $O^{\times}_{O}$, $Me^{\cdot}_{Me}$, $Me^{\cdot\cdot}_{i}$, $V^{\cdot\cdot}_{O}$, V''_{Me}, and O''_{i}. The first two entries are termed 'regular structural elements' and the last five are called 'irregular structural elements' or point defects in the ideal crystal lattice. The Kröger–Vink (1956) notation is used to indicate the atomic species, A, occupying a specific crystallographic site, S, and having an effective charge, C, relative to the ideal crystal lattice: A^{C}_{S}. In this nomenclature, the symbols $\times$, $\cdot$, and $'$ indicate neutral, one positive, and one negative effective charges. Vacant sites are denoted by a V, and ions located at interstitial sites are indicated by a subscript i. The defect $Me^{\cdot}_{Me}$ corresponds to a 3+ ion sitting at a site normally occupied by a 2+ ion, such as a ferric iron in a ferrous iron site. In a strict sense, charge neutrality is given by

$$\left[Me^{\cdot}_{Me}\right] + 2\left[V^{\cdot\cdot}_{O}\right] + 2\left[Me^{\cdot\cdot}_{i}\right] = 2[V''_{Me}] + 2[O''_{i}] \qquad [1a]$$

where the square brackets, [ ], indicate molar concentration. In a Mg-rich system, one possible disorder type is the combination of $Me^{\cdot\cdot}_{i}$ and V''_{Me} (Catlow *et al.*, 1994), such that the charge neutrality condition is approximated as

$$\left[Me^{\cdot\cdot}_{i}\right] = [V''_{Me}] \qquad [1b]$$

In contrast, in an Fe-rich quasi-binary material such as (Mg, Fe)O, likely majority point defects are $Fe^{\cdot}_{Me}$ and V''_{Me} (Hilbrandt and Martin, 1998), yielding the charge neutrality condition

$$\left[Fe^{\cdot}_{Me}\right] = 2[V''_{Me}] \qquad [1c]$$

where $Fe^{\cdot}_{Me}$ is often written as $h^{\cdot}$, indicating a highly mobile electron hole localized at a Fe^{2+} site.

To obtain expressions that give the dependences of point defect concentrations on thermodynamic variables such as temperature, pressure, and component activities, reaction equations are needed. The first reaction equation should involve the majority point defects. In the case of the disorder type given by eqn [1b], the appropriate reaction starts with a regular structural element resulting in

$$Me^{\times}_{Me} \rightleftarrows Me^{\cdot\cdot}_{i} + V''_{Me} \qquad [2]$$

for which the law of mass action yields

$$a_{Me^{\cdot\cdot}_{Me}} a_{V''_{Me}} = a_{Me^{\times}_{Me}} K_2 \qquad [3a]$$

where K_2 is the reaction constant for the reaction in eqn [2]. Since the activity of $Me^{\times}_{Me}$ is little affected by the presence of a small concentration of point defects (typically $<10^{-3}$), $a_{Me^{\times}_{Me}} \approx \left[Me^{\times}_{Me}\right] \approx 1$. Likewise, for ideally dilute solutions of point defects, the activities of the point defects can be replaced by their concentrations such that eqn [3a] becomes

$$\left[Me^{\cdot\cdot}_{i}\right][V''_{Me}] = K_2 = \exp\frac{-G_F}{RT} \qquad [3b]$$

where G_F is the Gibbs energy for the reaction in eqn [2] and RT has the usual meaning. This reaction describes the formation of the so-called Frenkel point defects (a vacancy–interstitial pair). If the charge neutrality condition in eqn [1b] and the mass action equation in eqn [3b] are combined, the dependence on temperature and pressure of the concentrations of the Frenkel defects is

$$\left[Me^{\cdot\cdot}_{i}\right] = [V''_{Me}] = \sqrt{K_2} = \exp\frac{-G_F}{2RT} \qquad [4]$$

Frenkel majority point defects are an example of a thermal disorder type, that is, the concentrations of these point defects depend on temperature and pressure but not on the activities of the components. A second example of thermal disorder occurs if Schottky point defects, V''_{Me} and $V^{\cdot\cdot}_{O}$, are the majority point defects.

For the disorder type given by eqn [1c], the appropriate reaction involves a regular structural element plus a neutral crystal component to yield

$$\frac{1}{2}O_2(\text{srg}) + 2Fe^{\times}_{Me} + Me^{\times}_{Me} \rightleftarrows 2Fe^{\cdot}_{Me} + V''_{Me} + MeO(\text{srg}) \qquad [5]$$

where the oxygen is provided from a site of repeatable growth (srg) such as a dislocation, grain boundary, or crystal–gas interface (surface). The law of mass action yields

$$\left[Fe^{\cdot}_{Me}\right]^2[V''_{Me}]a_{MeO} = \left[Fe^{\times}_{Me}\right]^2\left[Me^{\times}_{Me}\right]f_{O_2}^{1/2}K_5 \qquad [6]$$

where f_{O_2} is the oxygen fugacity. If the charge neutrality condition in eqn [1c] is now substituted into eqn [6] and the approximation $[Me^{\times}_{Me}] \approx a_{MeO} = 1$ is made, then

$$\begin{aligned}\left[Fe^{\cdot}_{Me}\right] &= 2[V''_{Me}] \\ &= \sqrt[3]{2}\left[Fe^{\times}_{Me}\right]^{2/3} f_{O_2}^{1/6} K_5^{1/3} \\ &= \sqrt[3]{2}\left[Fe^{\times}_{Me}\right]^{2/3} f_{O_2}^{1/6} \exp\frac{-G_5}{3RT}\end{aligned} \qquad [7]$$

Thus, if a neutral crystal component is added from a site of repeatable growth, the concentrations of the

majority point defects will depend not only on pressure and temperature but also on component activities, often referred to as an activity-dependent disorder type. In this case, it should be noted that the material will be non-stoichiometric with typically $[V''_{Me}] \gg [V^{\cdot\cdot}_{O}]$. Also, a comparison of eqn [4] with eqn [7] demonstrates that the form as well as the magnitude of the concentration of V''_{Me} depends on the charge neutrality condition.

Since $[V^{\cdot\cdot}_{O}]$ is generally several orders of magnitude smaller than $[V''_{Me}]$, O diffuses much more slowly than Me, at least through the interiors of grains. Consequently, as discussed below, the rate of diffusion creep (specifically, Nabarro–Herring creep) and of dislocation climb are limited by the rate of O diffusion. Hence, it is important to examine the dependence of the concentration of $V^{\cdot\cdot}_{O}$ on temperature, pressure, and oxygen fugacity. Since the dependence of the concentration of V''_{Me} on these parameters has been determined above, formulation of a reaction involving $V^{\cdot\cdot}_{O}$ and V''_{Me} provides a good starting point. The point defects $V^{\cdot\cdot}_{O}$ and V''_{Me} are related via the Schottky formation reaction

$$Me^{\times}_{Me} + O^{\times}_{O} \rightleftarrows V''_{Me} + V^{\cdot\cdot}_{O} + MeO \qquad [8]$$

It should be emphasized that it is essential in reaction equations such as eqn [8] that the number and identity of the atomic species, the crystallographic sites, and the effective charges (recall A^{C}_{S}) be the same on the two sides of the reaction equation. The law of mass action for eqn [8] reads

$$[V''_{Me}][V^{\cdot\cdot}_{O}] = K_8 = \exp\frac{-G_8}{RT} \qquad [9]$$

again using the approximations $a_{Me^{\times}_{Me}} \approx a_{O^{\times}_{O}} \approx 1$ with a_{MeO} equal to unity since MeO is present. For the Frenkel thermal disorder type given by eqn [1b], $[Me^{\cdot\cdot}_{i}] = [V''_{Me}]$, if eqn [9] is now combined with eqn [4], then

$$[V^{\cdot\cdot}_{O}] = [V''_{Me}]^{-1}K_8 = \frac{K_8}{\sqrt{K_2}} = \exp\frac{-(G_8 - G_F/2)}{RT} \qquad [10]$$

For the activity-dependent disorder type given by eqn [1c], $[Fe^{\cdot}_{Me}] = 2[V''_{Me}]$, if eqn [9] is combined with eqn [7], then

$$\begin{aligned}[V^{\cdot\cdot}_{O}] &= [V''_{Me}]^{-1}K_8 \\ &= \sqrt[3]{4}[Fe^{\times}_{Me}]^{-2/3} f_{O_2}^{-1/6}\frac{K_8}{K_5^{1/3}} \\ &= \sqrt[3]{4}[Fe^{\times}_{Me}]^{-2/3} f_{O_2}^{-1/6}\exp\frac{-(G_8 - G_5/3)}{RT}\end{aligned} \qquad [11]$$

Under hydrous conditions, additional point defects must be considered. Hydrogen ions, that is protons, $\dot{p}$ occupy interstitial sites, $H^{\cdot}_{i}$, near oxygen ions thus corresponding to the point defects $(OH)^{\cdot}_{O}$. This water-derived point defect can be introduced through dissociation of a water molecule by the reaction

$$H_2O(srg) + 2O^{\times}_{O} + Me^{\times}_{Me} \rightleftarrows 2(OH)^{\cdot}_{O} + V''_{Me} + MeO(srg) \qquad [12]$$

In addition, point defect associates such as those produced between $(OH)^{\cdot}_{O}$ and V''_{Me} can form

$$(OH)^{\cdot}_{O} + V''_{Me} \rightleftarrows \{(OH)^{\cdot}_{O} - V''_{Me}\}' \qquad [13]$$

where the curly brackets { } indicate a defect associate. This and other defect associates as well as $(OH)^{\cdot}_{O}$ must now be included in the charge neutrality equation, eqn [1]. New disorder types such as

$$[(OH)^{\cdot}_{O}] = \left[\{(OH)^{\cdot}_{O} - V''_{Me}\}'\right] \qquad [14]$$

and

$$[Fe^{\cdot}_{Me}] = \left[\{(OH)^{\cdot}_{O} - V''_{Me}\}'\right] \qquad [15]$$

must also be considered. A summary of the dependencies of the concentrations of various point defects on oxygen fugacity and water fugacity for the system MeO is provided in **Table 1** for a range of charge neutrality conditions.

2.14.2.1.2 Kinetics

Diffusion of atoms and ions through crystalline solids takes place by movement of point defects, namely, vacancies and self-interstitials. Here the discussion focuses on vacancies; a parallel analysis applies for self-interstitials. Since the fraction of vacant sites, X_V, on any specific sublattice is small, typically $<10^{-3}$ to $\ll 10^{-3}$, vacancies diffuse much more rapidly than the ions on that sublattice. From the point of view of a vacancy, all of the neighboring sites are available, while from the perspective of an ion, possibly one but more likely no sites are available at any particular moment. This connection between the movement of ions and that of vacancies leads to the following relationship between the diffusion coefficient for ions, D_{ion}, and that for vacancies, D_V:

$$X_{ion}D_{ion} = X_V D_V \qquad [16a]$$

where X_{ion} is the fraction of sites on a given sublattice occupied by the ions associated with that sublattice.

Table 1 Dependence of point defect concentrations on oxygen fugacity and water fugacity, expressed as the exponents p and q in the relationship $[\,] \propto f_{O_2}^{p} f_{H_2O}^{q}$, for several charge neutrality conditions for MeO

Charge neutrality	$Me_{Me}^{\cdot}$	V_{Me}''	$V_O^{\cdot}$	$\{Me_{Me}^{\cdot} - V_{Me}''\}'$	$(OH)_O^{\cdot}$	$\{(OH)_O^{\cdot} - V_{Me}''\}'$
$[Me_{Me}^{\cdot}] = 2[V_{Me}'']$	1/6, 0	1/6, 0	−1/6, 0	1/3, 0	−1/12, 1/2	1/12, 1/2
$[(OH)_O^{\cdot}] = 2[V_{Me}'']$	1/4, −1/6	0, 1/3	0, −1/3	1/4, 1/6	0, 1/3	0, 2/3
$[Me_{Me}^{\cdot}] = \left[\{(OH)_O^{\cdot} - V_{Me}''\}'\right]$	1/8, 1/4	1/4, −1/2	−1/4, 1/2	3/8, −1/4	−1/8, 3/4	1/8, 1/4
$[(OH)_O^{\cdot}] = \left[\{(OH)_O^{\cdot} - V_{Me}''\}'\right]$	1/4, 0	0, 0	0, 0	1/4, 0	0, 1/2	0, 1/2

Since $X_{ion} = (1 - X_V) \approx 1$, eqn [16a] is usually approximated as

$$D_{ion} \approx X_V D_V \qquad [16b]$$

such that

$$D_{ion} \ll D_V \qquad [16c]$$

that is, vacancies diffuse orders of magnitude faster than ions because $X_V \ll 1$.

One consequence of the rapid diffusion of vacancies (as well as of electron holes) is that equilibrium vacancy concentrations are attained relatively rapidly in response to changes in oxygen partial pressure or oxide activity, typically in much less than an hour under laboratory conditions for which diffusion distances are on the scale of the sample size (Mackwell *et al.*, 1988; Wanamaker, 1994). Point defect concentrations respond even more quickly to changes in temperature and pressure for which the appropriate diffusion length is the distance between sites of repeatable growth, which serve as sources and sinks for point defects.

The concentration of vacancies in a mineral will differ from one sublattice to the next. In a system composed of Me = (Mg, Fe), Si, and O, the concentration of vacancies on the Me sublattice is generally several orders of magnitude larger than the concentrations on the Si and O sublattices, that is, $[V_{Me}''] >> [V_O^{\cdot\cdot}]$, $[V_{Si}'''']$ (e.g., Nakamura and Schmalzried, 1983, 1984; Tsai and Dieckmann, 2002). As a result, $D_{Me} >> D_O$, D_{Si}.

For deformation by diffusion creep or dislocation climb processes, the flux of ions directly enters expressions for the strain rate. The deformation rate is calculated from analyses of the flux of ions between regions experiencing different stress states, such as between grain boundaries in a rock that are oriented normal to and those that are oriented parallel to the maximum principal stress. In an ionic solid, the fluxes of all of the constituent ions must be coupled in order to maintain stoichiometry (Ruoff, 1965; Readey, 1966; Gordon, 1973; Dimos *et al.*, 1988; Jaoul, 1990; Schmalzried, 1995, pp. 345–346). As a consequence, the creep rate of a monominerallic rock is controlled by the rate of diffusion of the slowest diffusing ion.

In the case of olivine, Me_2SiO_4, for diffusion along parallel paths (i.e., 1-D diffusion), the fluxes of Me^{2+}, Si^{4+}, and O^{2-} are given by (e.g., Schmalzried, 1981, p. 63; Schmalzried, 1995, pp. 78–82)

$$j_{Me^{2+}} = -\frac{D_{Me} C_{Me}}{RT}\frac{\partial \eta_{Me^{2+}}}{\partial \xi} = -\frac{D_{Me} C_{Me}}{RT}\left(\frac{\partial \mu_{Me^{2+}}}{\partial \xi} + 2F\frac{\partial \varphi}{\partial \xi}\right) \qquad [17a]$$

$$j_{Si^{4+}} = -\frac{D_{Si} C_{Si}}{RT}\frac{\partial \eta_{Si^{4+}}}{\partial \xi} = -\frac{D_{Si} C_{Si}}{RT}\left(\frac{\partial \mu_{Si^{4+}}}{\partial \xi} + 4F\frac{\partial \varphi}{\partial \xi}\right) \qquad [17b]$$

and

$$j_{O^{2-}} = -\frac{D_O C_O}{RT}\frac{\partial \eta_{O^{2-}}}{\partial \xi} = -\frac{D_O C_O}{RT}\left(\frac{\partial \mu_{O^{2-}}}{\partial \xi} - 2F\frac{\partial \varphi}{\partial \xi}\right) \qquad [17c]$$

where j is the flux, D the self-diffusivity, C the concentration, and η the electrochemical potential of the appropriate ionic species. The electrochemical potentials for the various ions are written in terms of the chemical potential, μ, and the electrical potential, φ, as (e.g., Schmalzried, 1981, p. 63)

$$\eta = \mu + zF\varphi \qquad [18]$$

where z is the charge on the ion and F is the Faraday constant. To maintain stoichiometry during diffusion-controlled creep in which transport of entire lattice molecules must occur between sites of repeatable growth such as dislocations and grain boundaries, the flux coupling condition is

$$\frac{j_{Me^{2+}}}{C_{Me}} = \frac{j_{Si^{4+}}}{C_{Si}} = \frac{j_{O^{2-}}}{C_O} \qquad [19a]$$

Equation [19a] applies specifically to the case in which the all of the ions diffuse along a single path or parallel paths; the more general case in which diffusion occurs along multiple paths (e.g., along grain boundaries and through grain interiors) is treated in Dimos *et al.* (1988; see also Kohlstedt, 2006).

The flux coupling equation provides a means of eliminating the $\partial\varphi/\partial\xi$ term from the flux equations. The flux coupling condition for olivine in eqn [19a] can be rewritten as

$$2j_{Me^{2+}} = 4j_{Si^{4+}} = j_{O^{2-}} \qquad [19b]$$

Then, since $D_{Me} >> D_O > D_{Si}$, the approximation

$$\frac{\partial\eta_{Me^{2+}}}{\partial\xi} = \frac{\partial\mu_{Me^{2+}}}{\partial\xi} + 2F\frac{\partial\varphi}{\partial\xi} \approx 0 \qquad [20]$$

must hold in order to satisfy the flux coupling condition given by eqn [19b]. Using the implicit assumption of local thermodynamic equilibrium, the chemical potentials of the ions can be written in terms of the chemical potentials of the oxides as

$$\mu_{Me^{2+}} + \mu_{O^{2-}} = \mu_{MeO} \qquad [21a]$$

and

$$\mu_{Si^{4+}} + 2\mu_{O^{2-}} = \mu_{SiO_2} \qquad [21b]$$

Thus, the flux coupling condition in eqn [19b] leads to the relation

$$D_{Si}\frac{\partial\mu_{SiO_2}}{\partial\xi} = (D_O + 2D_{Si})\frac{\partial\mu_{MeO}}{\partial\xi} \qquad [22]$$

The flux of Si^{4+}, the slowest ionic species, then becomes

$$j_{Si^{4+}} = -\frac{C_{Si}D_{Si}}{RT}\left(\frac{\partial\mu_{SiO_2}}{\partial\xi} - 2\frac{\partial\mu_{MeO}}{\partial\xi}\right) \qquad [23a]$$

Since the chemical potential of olivine is

$$\mu_{Me_2SiO_4} = 2\mu_{MeO} + \mu_{SiO_2}$$

the flux of Si^{4+} is

$$j_{Si^{4+}} = -\frac{C_{Si}D_{Si}}{RT}\frac{D_O}{D_O + 4D_{Si}}\frac{\partial\mu_{Me_2SiO_4}}{\partial\xi} \qquad [23b]$$

The chemical potential of olivine contains an activity, a, and a stress, σ, term such that

$$\frac{\partial\mu_{Me_2SiO_4}}{\partial\xi} = RT\frac{\partial\ln a_{Me_2SiO_4}}{\partial\xi} - V_{Me_2SiO_4}\frac{\partial\sigma}{\partial\xi} \qquad [24]$$

where $V_{Me_2SiO_4}$ is the molar volume of olivine (e.g., Ready, 1966; Gordon, 1973; Dimos *et al.*, 1988; Schmalzried, 1995, p. 334). The first term on the right-hand side of eqn [24] can be expressed in terms of the gradient in the concentration of vacancies on the Me sublattice (Dimos *et al.*, 1988; Jaoul, 1990) as

$$RT\frac{\partial\ln a_{Me_2SiO_4}}{\partial\xi} \approx -2RT\frac{\partial[V''_{Me}]}{\partial\xi} \approx -2[(V''_{Me})^o]V_{Me_2SiO_4}\frac{\partial\sigma}{\partial\xi} \qquad [25]$$

where $[(V''_{Me})^o]$ is the concentration of Me vacancies under hydrostatic stress conditions. The gradient in the concentration in metal vacancies results from the gradient in normal stress between sources for vacancies (regions of minimum compressive stress) and sinks for vacancies (regions of maximum compressive stress). Since $[(V''_{Me})^o]$ is small, $<10^{-3}$, the second term in eqn [24] dominates such that

$$\frac{\partial\mu_{Me_2SiO_4}}{\partial\xi} \approx -V_{Me_2SiO_4}\frac{\partial\sigma}{\partial\xi} \qquad [26]$$

Therefore, if $D_O >> D_{Si}$

$$j_{Si^{4+}} = \frac{C_{Si}D_{Si}}{RT}V_{Me_2SiO_4}\frac{\partial\sigma}{\partial\xi} \qquad [27]$$

2.14.2.2 Line Defects – Structure and Dynamics

Dislocations are line defects that separate regions of a crystal that have slipped from those that have not slipped. Their motion by glide and climb is central to deformation of most crystalline solids, much like point defects are essential for diffusion. Unlike point defects, dislocations are not equilibrium defects. While the change in enthalpy associated with the formation of a dislocation is quite large, the change in entropy is relatively small. In a simplistic analogy, the former might be considered equal to the change in enthalpy due to the formation of of N vacancies, where the vacancies form a row of the same length as the dislocation line. In contrast, the change in entropy resulting from the formation of N vacancies constrained to lie along a line will be significantly less than that associated with the formation of N vacancies randomly distributed in a crystal. The result is that, at equilibrium, a crystal is expected to be dislocation free (Devereux, 1983, pp. 368–372).

A dislocation is characterized by two vector quantities, its line direction, ℓ, which defines the direction of the dislocation at each point along its length, and a displacement or Burgers vector, **b**, which defines the displacement of the lattice produced as the dislocation moves through a crystal. For a dislocation loop such as illustrated in **Figure 1**, the tangential line

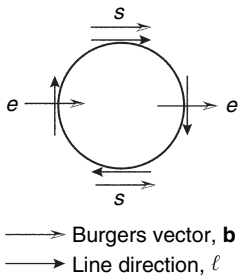

Figure 1 Sketch of dislocation loop indicating the direction of the Burgers vector, **b**, and of the dislocation line, ℓ, at each point along the loop. The edge and screw segments of the dislocation loop are denoted by *e* and *s*, respectively.

direction changes from one point to the next along the loop, while the Burgers vector is the same at every point. Regions along the dislocation loop for which **b** is perpendicular to ℓ are termed edge segments, while regions for which **b** is parallel to ℓ are termed screw segments. Regions of a dislocation for which **b** and ℓ are neither perpendicular nor parallel are referred to as mixed segments.

Movement of a dislocation can take place by glide and climb. An edge dislocation can move in one of two ways. If an edge dislocation moves in the glide plane defined by $\mathbf{b} \times \ell$, its motion is conservative. In contrast, if an edge dislocation moves normal to its glide plane, the process is nonconservative in that lattice molecules are added to or taken away from the dislocation line by diffusion such that the dislocation climbs out of its glide plane. A screw dislocation does not have a specific glide plane since **b** and ℓ are parallel to each other. Hence, a screw dislocation generally glides on the plane that offers least resistance to its motion. If it encounters an obstacle to its movement, a screw dislocation can cross slip off of its original glide plane onto a parallel glide plane in order to continue moving. A dislocation must always move in a direction perpendicular to its line direction. The displacement resulting from glide of an edge dislocation is thus parallel to the direction of dislocation glide, while the displacement resulting from movement of a screw dislocation is perpendicular to its direction of motion defined by the velocity vector, **v**, as illustrated in **Figure 2**. Finally, a slip system is defined for a dislocation by the combination of a unit vector normal to the slip plane, **n**, and **b**. As an example, important slip systems in clinopyroxene include $\{110\}\ \langle 1\bar{1}0\rangle$, $\{110\}[001]$, and $(100)[001]$ (Bystricky and Mackwell, 2001). Slip systems in olivine include $(010)[100]$, $(001)[100]$, $(100)[001]$, and $(010)[001]$ with the dominate slip system determined by stress, water concentration, as well as pressure and temperature conditions (Carter and Avé Lallemant, 1970; Jung and Karato, 2001; Mainprice *et al.*, 2005).

To first order, dislocations with short displacement vectors are preferred over those with longer displacement vectors since the energy per unit length of a dislocation, E_{disl}, is proportional to the square of the Burgers vector. For an edge dislocation in an elastically isotropic material (Weertman and Weertman, 1992, pp. 45–52)

$$E_{\text{disl}} = \frac{Gb^2}{4\pi(1-v)} \ln \frac{r}{r_c} \qquad [28]$$

where G is the shear modulus, r is the mean spacing between dislocations, and r_c is the radius of the dislocation core. In eqn [28], the contribution of the core of the dislocation to the elastic strain energy has been neglected. For elastically anisotropic materials, the full matrix of elastic constants must be considered, as discussed in detail by Hirth and Lothe (1968, pp. 398–440).

Slip generally occurs on the closest packed plane that contains **b**, that is, the most widely separated

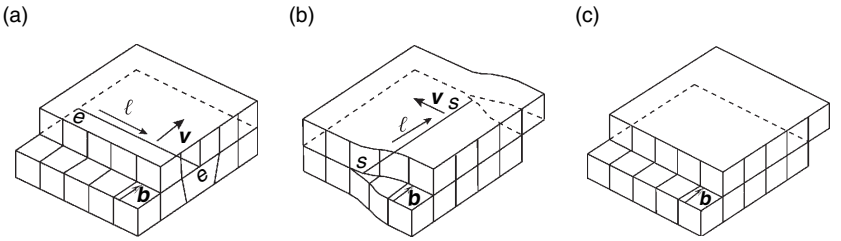

Figure 2 Sketch illustrating that (a) the movement of an edge dislocation, *e*, and (b) the movement of a screw dislocation, *s*, with the same Burgers vector (c) produce the same displacement of the upper half of a crystal relative to the lower half. Adapted from Kelly A and Groves GW (1970) *Crystallography and Crystal Defects*, 428 pp. Reading, MA: Addison-Wesley Publishing Company.

planes and thus, in general, the most weakly bonded planes. In olivine, $|[100]| < |[001]| < |[010]|$ suggesting that $\mathbf{b} = [100]$ should dominate. However, plastic deformation of a polycrystalline material cannot proceed without opening up void space if only one or two independent slip systems operate. Homogeneous plastic deformation of a rock requires dislocation glide on five independent slip systems (von Mises, 1928). This constraint is relaxed to glide on four independent slip systems if deformation is allowed to be heterogeneous (Hutchinson, 1976). If dislocations both glide and climb, homogeneous deformation necessitates the operation of just three independent slip systems (Kelly and Groves, 1969). Processes such as grain-boundary sliding, ionic diffusion, and twinning can also relax the von Mises criterion.

Glide and climb of dislocations involve steps along the dislocation line. Steps that lie in the glide plane, kinks, facilitate glide. Steps out of the glide plane, jogs, facilitate climb.

Dislocations interact with one another and with an applied stress field through the stress field that arises due to the elastic distortion caused by the presence of each dislocation. The stress fields associated with edge and screw dislocations in an elastically isotropic and elastically anisotropic media are derived in Hirth and Lothe (1968, pp. 398–440) and in Weertman and Weertman (1992, pp. 22–41). The force on a dislocation is then calculated using the Peach–Koehler equation (Peach and Koehler, 1950). In its simplest form, the force per unit length, f, on a dislocation is

$$f = \sigma b \qquad [29]$$

where the stress σ arises, for example, from a neighboring dislocation or an external force.

2.14.2.3 Planar Defects – Structure and Energy

Planar defects include twin boundaries, stacking faults, grain boundaries, and interphase boundaries. The emphasis in this chapter is on grain boundaries and interphase boundaries, because of the important role of these two types of interfaces in plastic deformation.

If the misorientation across a grain boundary is not too large, say, <15° (i.e., a low-angle boundary), the interface can be constructed from a periodic array of dislocations. A low-angle tilt boundary consists of a series of parallel edge dislocations, as illustrated schematically in **Figure 3** and imaged in **Figure 4**. In the case of a low-angle tilt boundary, the spacing between dislocations, h, can be expressed in terms of the misorientation angle, ϑ, across the boundary as

$$h = \frac{b}{2\sin(\vartheta/2)} \qquad [30a]$$

For a small misorientation, the misorientation angle can be approximated by

$$\vartheta \approx \frac{b}{h} \qquad [30b]$$

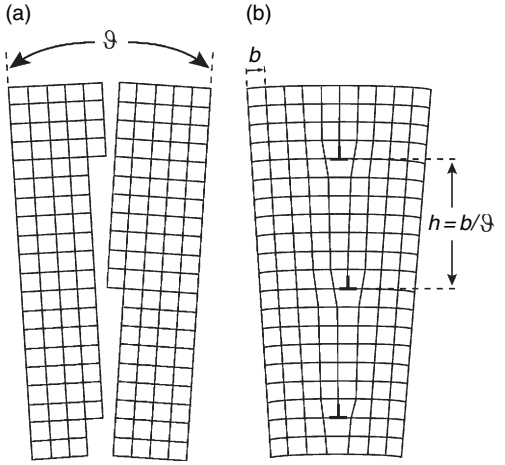

Figure 3 Sketch of a low-angle tilt boundary formed by a series of periodically spaced edge dislocations, which are denoted by the inverted 'T' symbols. Adapted from Read WT Jr (1953) *Dislocation in Crystals*, 175pp. New York: McGraw-Hill Book Company.

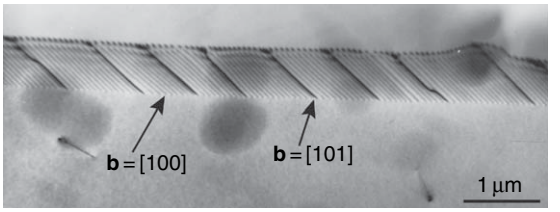

Figure 4 Bright-field transmission electron micrograph of a low-angle tilt boundary in olivine. Two sets of dislocations, one with $\mathbf{b} = [100]$ and the other with $\mathbf{b} = [101]$, are present in this boundary. The darker $\mathbf{b} = [101]$ dislocations are more widely spaced than the lighter, periodically spaced $\mathbf{b} = [100]$ dislocations. This image was taken with the diffraction condition $\mathbf{g} = (002)$, hence the $\mathbf{b} = [100]$ dislocations exhibit only residual contrast. Adapted from Goetze C and Kohlstedt DL (1973) Laboratory study of dislocation climb and diffusion in olivine. *Journal of Geophysical Research* 78: 5961–5971.

Starting with eqn [28], the elastic strain energy per unit area of a low-angle tilt boundary can then be derived (Read and Shockley, 1950)

$$E_{\text{tilt}} = \frac{Gb^2}{4\pi(1-v)}\frac{\vartheta}{b}(A - \ln\vartheta) \qquad [31]$$

where the parameter A accounts for the fraction of the elastic strain energy associated with the cores of the dislocations. Once the cores of the dislocations in a tilt boundary begin to overlap, this simple description of a grain boundary breaks down.

A low-angle twist boundary requires two, generally orthogonal, sets of screw dislocations. The elastic energy per unit area for a low-angle twist boundary is similar to that for a low-angle tilt boundary. A sketch of the atomic structure of a low-angle twist boundary formed by rotating the lattices of two grains relative to each through an angle ϑ, thus forming orthogonal sets of dislocations, is presented in **Figure 5**. A transmission electron micrograph of a twist boundary is shown in **Figure 6**.

As illustrated in **Figure 7**, grain-boundary energy increases rapidly with increasing ϑ, as described by eqn [31], up to $\vartheta \approx 20°$. At larger values of ϑ, grain-boundary energy is approximately constant except for a few minima that occur at specific orientations. Other than twin boundaries, these minima occur at orientations for which a significant fraction of the lattice points in the two neighboring grains are nearly coincident (Chan and Balluffi, 1985, 1986). A simple example of this coincidence structure illustrating the type of periodicity that can be present in specific grain boundaries is shown in **Figure 8** for a twist boundary.

Grain and interphase boundaries influence the physical properties of rocks in several important ways. First, grain-boundary sliding provides a mechanism for producing strain in response to an applied differential stress. Grain-boundary sliding takes place by the movement of grain-boundary dislocations. As discussed in the next section, grain-boundary sliding is a critical part of diffusion creep (Raj and Ahsby, 1971). Grain-boundary sliding can also be important during deformation in which dislocation glide and climb operate (e.g., Langdon, 1994). In this case, lattice dislocations can dissociate and enter grain boundaries resulting in enhanced or stimulated grain-boundary sliding (Pshenichnyuk *et al.*, 1998). As discussed below, grain-boundary sliding often provides an additional mechanism of deformation and can be particularly important in rocks composed of minerals with fewer than five independent slip systems.

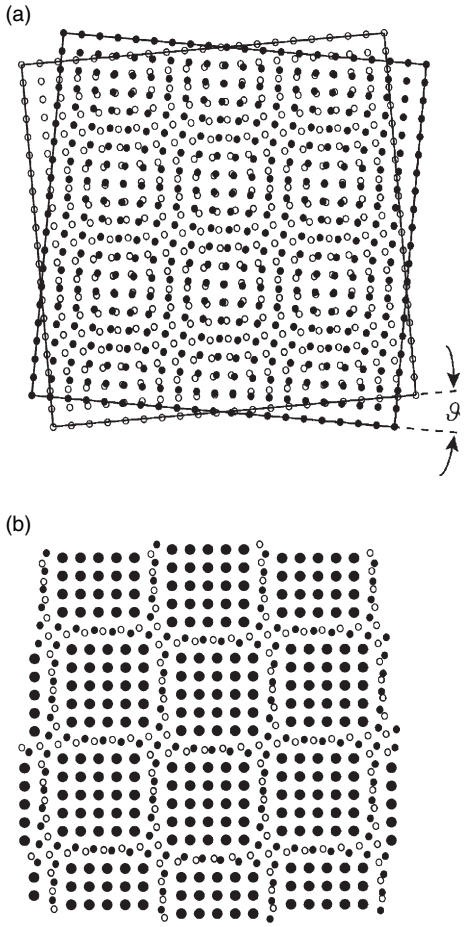

Figure 5 Sketch of atomic configuration for a [001] low-angle twist boundary in a simple cubic lattice with the boundary parallel to the plane of the figure. In this example, $\vartheta \approx 10°$. (a) In the unrelaxed atomic configuration, the open circles represent atoms in the plane just above the boundary, while the closed circles represent the atoms in the plane just below the boundary. (b) In the relaxed atomic configuration, the grains join in regions in which the atomic match is good with two orthogonal sets of screw dislocations located between these regions. Adapted from Schmalzried H (1995) *Chemical Kinetics of Solids*, 433pp. New York: VCH Publishers.

Second, grain boundaries migrate in response to a difference in dislocation density between neighboring grains. As expressed in eqn [28], each dislocation introduces elastic strain energy into a crystalline grain. If during deformation the dislocation density becomes higher in one grain than in the next grain, a thermodynamic driving force exists that can cause the grain boundary to migrate toward the region of higher dislocation density, absorbing lattice dislocations into the grain boundary thus reducing the

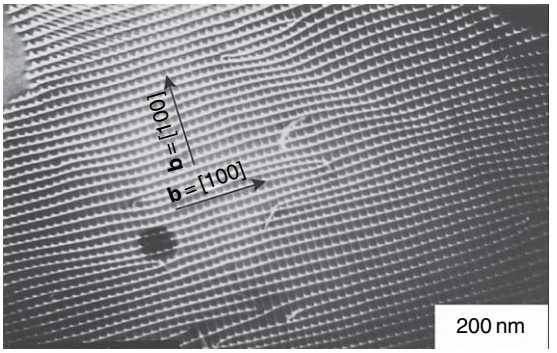

Figure 6 Dark-field transmission electron micrograph of two orthogonal sets of screw dislocations, one with **b** = [100] and the other with **b** = [001], forming a low-angle twist boundary in the (010) plane of olivine. The boundary is very nearly parallel to the plane of the figure. Adapted from Ricoult DL and Kohlstedt DL (1983a) Structural width of low-angle grain boundaries in olivine. *Physics and Chemistry of Minerals* 9: 133–138. Ricoult DL and Kohlstedt DL (1983b) Low-angle grain boundaries in olivine. In: Yan MF and Heuer AH (eds.) *Advances in Ceramics*, *Character of Grain Boundaries*, vol. 6, pp. 56–72. Columbus: American Ceramic Society.

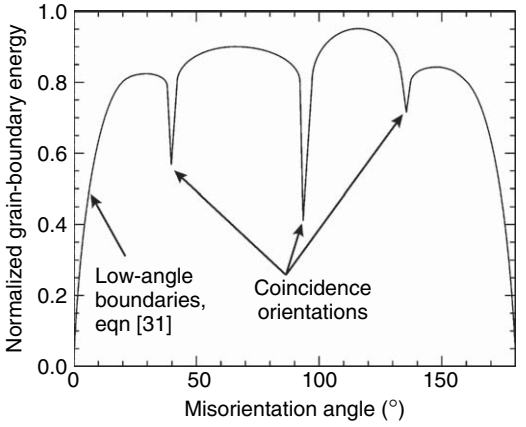

Figure 7 Sketch of normalized grain-boundary energy vs misorientation angle illustrating the energy minima that arise when the two neighboring grains are oriented such that a significant fraction of lattice sites are coincident.

stored strain energy. A dislocation-free region is left in the wake of the migrating boundary.

Third, grain boundaries are short-circuit paths for diffusion. The rate of diffusion along a grain boundary is in general several orders of magnitude faster than through a grain interior (Shemon, 1983, pp. 164–175). Thus, even though the cross-sectional area of a grain boundary is small relative to that of the grain itself, the flux of atoms passing through a grain boundary can be significant. The result is that, in the diffusion creep regime, grain-boundary diffusion is often the primary

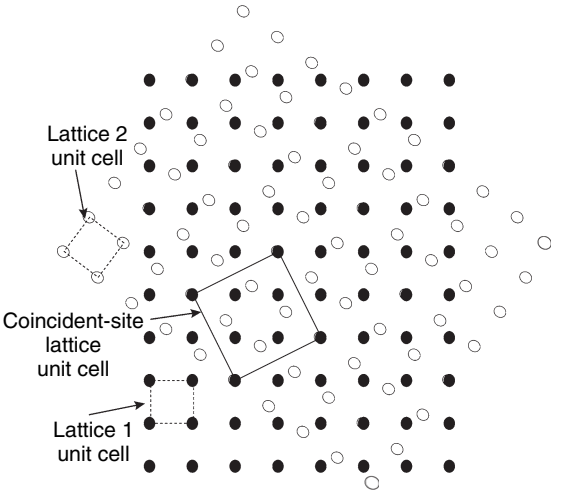

Figure 8 Sketch of lattice sites in two simple cubic grains that have been rotated relative to each other by ~53°. At this orientation, a fraction of the lattice sites from the two grains coincide forming a coincident-site lattice with a unit cell that is larger than those of the two adjoining grains.

mechanism for deformation. It should also be noted that grain boundaries provide storage sites for elements that, due to size or charge, are incompatible in the grain interior (Hiraga *et al.*, 2003, 2004, 2007; Hiraga and Kohlstedt, 2007). The presence of incompatible elements at grain and interphase boundaries perturbs the structure and the local charge state of the boundary, which in turn can affect diffusion kinetics (Mishin and Herzi, 1999).

2.14.3 Mechanisms of Deformation and Constitutive Equations

The mechanism of deformation that dominates the plastic deformation of a rock depends both on the properties of the rock such as grain size, d, and phase content, Φ, and on thermodynamic parameters such as temperature, pressure, P, water fugacity, and component (oxide) activity, a_{ox}. The dependence of strain rate, $\dot{\varepsilon}$, on these quantities can be expressed in a general constitutive equation or flow law as

$$\dot{\varepsilon} = \dot{\varepsilon}(d,\ \Phi,\ T,\ P,\ f_{H_2O},\ a_{ox},\ \ldots) \qquad [32]$$

Diffusion-controlled creep tends to be important at low differential stresses in fine-grained rocks. In contrast, dislocation-dominated processes govern flow at higher stresses in coarser-grained rocks. In this section, some of the constitutive equations used to describe flow in the diffusion and dislocation

deformation regimes are first introduced. Then, the influence on rheological behavior of two important fluids, water and melt, are discussed.

2.14.3.1 Constitutive Equations

2.14.3.1.1 Diffusion creep

Diffusion creep can be divided into two regimes, one in which diffusion through the interiors of grains controls the rate of deformation (Nabarro, 1948; Herring, 1950) and the other in which diffusion along grain boundaries governs the rate of deformation (Coble, 1963). The relative importance of these two mechanisms depends primarily on grain size and temperature.

2.14.3.1.1.(i) Grain matrix diffusion The rate of deformation in the Nabarro–Herring creep regime in which diffusion through grain interiors limits the rate of creep is described by the relation (Nabarro, 1948; Herring, 1950)

$$\dot{\varepsilon}_{\mathrm{NH}} = \alpha_{\mathrm{NH}} \frac{\sigma V_{\mathrm{m}}}{RT} \frac{D_{\mathrm{gm}}}{d^2} \qquad [33]$$

where α_{NH} is a geometrical term and D_{gm} is the diffusion coefficient for the slowest species diffusing through the grain matrix (gm), that is, the grain interior. The important points to note are that strain rate is linearly proportional to the differential stress, inversely proportional to the square of the grain size, and exponentially dependent on temperature and pressure through the diffusion coefficient since

$$\begin{aligned} D_{\mathrm{gm}} &= D^{\mathrm{o}}_{\mathrm{gm}} \exp\left(-\frac{\Delta E_{\mathrm{gm}} + P\Delta V_{\mathrm{gm}}}{RT}\right) \\ &= D^{\mathrm{o}}_{\mathrm{gm}} \exp\left(-\frac{\Delta H_{\mathrm{gm}}}{RT}\right) \end{aligned} \qquad [34]$$

where $D^{\mathrm{o}}_{\mathrm{gm}}$ is a material-dependent parameter and ΔE_{gm}, ΔV_{gm}, and ΔH_{gm} are the activation energy, activation volume, and activation enthalpy for grain matrix diffusion, respectively.

2.14.3.1.1.(ii) Grain-boundary diffusion A similar expression applies in the Coble creep regime in which the creep rate is limited by diffusion through grain boundaries (Coble, 1963):

$$\dot{\varepsilon}_{\mathrm{C}} = \alpha_{\mathrm{C}} \frac{\sigma V_{\mathrm{m}}}{RT} \frac{\delta D_{\mathrm{gb}}}{d^3} \qquad [35]$$

where α_{C} is a geometrical term, δ is the diffusion width of the grain boundary, which is approximately equal to the structural width of ~1 nm (e.g., Atkinson, 1985; Carter and Sass, 1981; Ricoult and Kohlstedt, 1983a, 1983b), and D_{gb} is the diffusion coefficient for the slowest species diffusing along the boundaries. For grain boundaries

$$\begin{aligned} D_{\mathrm{gb}} &= D^{\mathrm{o}}_{\mathrm{gb}} \exp\left(-\frac{\Delta E_{\mathrm{gb}} + P\Delta V_{\mathrm{gb}}}{RT}\right) \\ &= D^{\mathrm{o}}_{\mathrm{gb}} \exp\left(-\frac{\Delta H_{\mathrm{gb}}}{RT}\right) \end{aligned} \qquad [36]$$

where $D^{\mathrm{o}}_{\mathrm{gb}}$ is a material-dependent parameter and ΔE_{gb}, ΔV_{gb}, and ΔH_{gb} are the activation energy, activation volume, and activation enthalpy for grain-boundary diffusion, respectively. Again, the strain rate increases linearly with increasing differential stress and increases exponentially with inverse temperature while decreasing exponentially with increasing pressure. However, in contrast to the Nabarro–Herring case, strain rate for Coble creep varies inversely as the cube, rather than the square, of the grain size.

Comparison of eqn [33] with eqn [35] reveals the following points: (1) Both creep mechanisms give rise to Newtonian viscous behavior ($\dot{\varepsilon} \propto \sigma^1$) with viscosity, $\eta \equiv \sigma/\dot{\varepsilon}$, independent of stress. (2) As long as the grain size is small enough that diffusion creep dominates over dislocation creep, Nabarro–Herring creep ($\dot{\varepsilon} \propto 1/d^2$) is more important than Coble creep ($\dot{\varepsilon} \propto 1/d^3$) at larger grain sizes. (3) Nabarro–Herring creep dominates at higher temperatures and Coble creep at lower temperatures because $\Delta H_{\mathrm{gb}} < \Delta H_{\mathrm{gm}}$.

The analyses of Nabarro (1948) and Herring (1950) and of Coble (1963) strictly apply to deformation of a single spherical grain. Subsequent analyses pointed out the necessity of grain-boundary sliding in diffusion creep of polycrystalline materials (Liftshitz, 1963; Raj and Ashby, 1971). The fact that grains tend to be equiaxed in samples deformed in the diffusion creep field indicates that grain-boundary sliding and grain rotation are crucial. The creep process is essentially that of grain-boundary sliding accommodated by diffusion both through grain interiors and along grain boundaries, if grain boundaries are too weak to a support shear stress. For this case, $\alpha_{\mathrm{NH}} = 14$ and $\alpha_{\mathrm{C}} = 14\pi$. Since grain-boundary and grain-matrix diffusion are independent/parallel processes, eqn [33] and [35] can be combined to give

$$\dot{\varepsilon}_{\mathrm{diff}} = 14\left(\frac{\sigma V_{\mathrm{m}}}{RT}\right)\left(D_{\mathrm{gm}} + \frac{\pi\delta D_{\mathrm{gb}}}{d}\right)\left(\frac{1}{d^2}\right) \qquad [37]$$

In general, this deformation mechanism is referred to simply as diffusion creep.

2.14.3.1.2 Deformation involving dislocations

As differential stress and/or grain size increases, a transition occurs from diffusion creep to dislocation-dominated deformation. One estimate of the stress required to move from the diffusion creep regime to the dislocation creep regime is based on a calculation of the stress required to operate a Frank–Reed dislocation source, σ_{FR}, (Frank and Read, 1950) and thus generate the dislocations necessary to sustain deformation:

$$\sigma_{FR} \approx \frac{2Gb}{L} \quad [38]$$

where L is the length of the dislocation segment operating as the source of new dislocations. If, the length of a dislocation line is limited by the grain size, then for $G = 70\,\text{GPa}$, $b = 0.5\,\text{nm}$, and $L = d = 10\,\mu\text{m}$, $\sigma_{FR} \approx 7\,\text{MPa}$

The strain produced by a single dislocation moving across a grain is very small, thus many dislocations must be generated and move to accomplish a significant amount of deformation. The strain, ε, produced in a cubic grain of dimension d by one dislocation moving through the grain is

$$\varepsilon = \frac{b}{d} \quad [39]$$

Thus, if $d = 1\,\text{mm}$, $\varepsilon \approx 5 \times 10^{-7}$. Greater strain is achieved by moving a larger number of dislocations through the grain. The density of dislocations, ρ, scales with applied differential stress as

$$\rho \approx \left(\frac{\sigma}{Gb}\right)^2 \quad [40]$$

such that $\rho \approx 10^9\,\text{m}^{-2}$ for a differential stress of 1 MPa. The strain produced by this density of dislocation moving a distance x is

$$\varepsilon = \rho b x \quad [41]$$

For $x = d$, $\varepsilon \approx 5 \times 10^{-4}$ (still a small value). To produce geologically significant strains, dislocations must be generated, move through crystalline grains, and then be removed so that new dislocations can be generated to maintain an approximately constant density of dislocations and keep the deformation process going. If steady-state deformation is attained, then a balance must be achieved, and one step in this series of steps will limit the rate of deformation.

A number of models have been proposed to describe the rate of deformation in terms of applied stress, temperature, pressure, and other thermodynamic and structural variables (e.g., Poirier, 1985, pp. 94–144; Evans and Kohlstedt, 1995). In the present chapter, characteristic elements of these models are reviewed in order to provide a framework for examining laboratory-determined deformation data and extrapolating to geological conditions.

The dependence of the rate of deformation accomplished by dislocation processes on differential stress can be examined through the Orowan equation, which is obtained by differentiating eqn [41] with respect to time and noting that in steady state the dislocation density is independent of time, $\partial\rho/\partial t = 0$ (Orowan, 1940; Poirier, 1985, pp. 62–63):

$$\dot{\varepsilon} = \rho b \bar{v} \quad [42]$$

where $\bar{v}$ is the average dislocation velocity. It should be noted, however, that the $\partial\rho/\partial t$ term is critical when discussing transient deformation (e.g., deformation immediately following a change in stress). As discussed in reference to eqn [40], the dislocation density is proportional to approximately the square of the stress, such that $\dot{\varepsilon} \propto \rho \propto \sigma^2$. Additional dependence of strain rate on differential stress enters through the dislocation velocity term.

In this discussion, dislocation creep is divided into three regimes. As with diffusion creep, the main parameters determining the relative importance of the various dislocation creep mechanisms are differential stress, temperature, pressure, and grain size. First, at high temperature (low stress) and relatively large grain size, all of the strain can be accomplished by glide and climb of dislocations. These conditions define the dislocation creep regime. Second, at high temperature but smaller grain size, grain-boundary sliding operates in conjunction with dislocation processes to produce strain. These conditions define a regime in which dislocation processes are accommodated by grain-boundary sliding, simply referred to here as the grain-boundary sliding regime. Third, at low temperatures (high stresses), deformation takes place by dislocation glide limited by the intrinsic resistance of the lattice. These conditions delineate the low-temperature plasticity regime.

2.14.3.1.2.(i) Dislocation creep To date, by far the majority of analyses of plastic deformation in geological materials have used a power-law equation

to describe experimental results. A general form of this flow law is

$$\dot{\varepsilon} = A\frac{\sigma^n}{d^m} f_{O_2}^p f_{H_2O}^q \exp - \frac{Q_{cr}}{RT} \quad [43]$$

where A is a material-dependent parameter and Q_{cr} is the activation energy (strictly, enthalpy) for creep. The power-law form of the creep equation arises by considering the role of dislocation climb and grain-boundary sliding in the deformation process.

The potential importance of dislocation climb as the rate-controlling step of high-temperature, steady-state creep was suggested in the early 1950s by Mott (1951, 1953, 1956). Subsequently, several climb-controlled creep models were developed that relate strain rate to differential stress and temperature, the latter though the self-diffusivity (for reviews see, e.g., Weertman (1978), Poirier (1985, pp. 94–144), Cannon and Langdon (1988), Evans and Kohlstedt (1995), and Weertman (1999)). The rate of climb of edge dislocations depends directly on diffusive fluxes of ions (e.g., Hirth and Lothe, 1968, pp. 506–519; Poirier, 1985, pp. 58–62). The justification for emphasizing the importance of climb in high-temperature ($T > (2/3)T_m$, where T_m is the melting temperature) deformation of crystalline materials is the observed one-to-one correlation between the activation energy for creep and the activation energy for self-diffusion of the slowest ionic species. This correlation has been observed for a large number of metallic and ceramic materials (e.g., Dorn, 1956; Sherby and Burke, 1967; Mukerjee *et al.*, 1969; Takeuchi and Argon, 1976; Evans and Knowles, 1978) as well as for olivine (Dohmen *et al.*, 2002; Chakraborty and Costa, 2004; Kohlstedt, 2006).

Two climb-based models of dislocation creep merit particular attention because of their pioneering contributions in this area and because they incorporate most of the elements found in subsequent models. Weertman (1955, 1957a) developed a flow law for steady-state dislocation creep in which dislocation glide produces the strain but dislocation climb controls the stain rate. In this model, a dislocation source generates a dislocation loop that expands by gliding until it encounters an obstacle such as a dislocation loop that was generated on a parallel glide plane. The two dislocations interact to form a dipole that prevents further glide until the two dislocations comprising the dipole climb to annihilate one another. Once the dipole is annihilated, the dislocation sources produce new dislocation loops (i.e., dislocation multiplication) to continue the deformation process. If glide is rapid and climb is slow then the average dislocation velocity is

$$\bar{v} = \frac{\ell_g + \ell_c}{t_g + t_c} \approx \frac{\ell_g}{\ell_c} v_c \quad [44]$$

where ℓ_g is the glide distance, ℓ_c is the climb distance, and v_c is the climb velocity (Poirier, 1985, p. 110; Weertman, 1999). The climb velocity, which is determined by diffusion of the slowest atomic/ionic species, is given by the expression (Hirth and Lothe, 1968, pp. 506–519)

$$v_c = 2\pi\frac{\sigma V_m}{RT}\frac{D}{b}\frac{1}{\ln(R_o/r_c)} \quad [45]$$

where the average spacing between dislocations, R_o, is usually written in terms of the dislocation density as $R_o \approx 1/\sqrt{\rho}$, and the inner cutoff (core) radius, r_c, is generally set at $r_c \approx b$. A flow law is then obtained by inserting eqn [40] and [45] into the Orowan equation, eqn [42], to yield (Weertman, 1999)

$$\dot{\varepsilon} = 2\pi\frac{GV_m}{RT}\left(\frac{\sigma}{G}\right)^3\frac{D}{b^2}\frac{1}{\ln(G/\sigma)}\frac{\ell_g}{\ell_c} \quad [46]$$

Nabarro (1967) formulated a model for steady-state dislocation creep based solely on dislocation climb. Bardeen–Herring sources (Bardeen and Herring, 1952) generate dislocations that form a network and continuously climb. Dislocation multiplication occurs by operation of dislocation sources thus increasing their density, while climb of dislocations of opposite sign toward one another results in annihilation thus decreasing their density. A balance between multiplication and annihilation results in steady-state creep described by the flow law (Nabarro, 1967; Nix *et al.*, 1971)

$$\dot{\varepsilon} = 2\frac{GV_m}{RT}\left(\frac{\sigma}{G}\right)^3\frac{D}{b^2}\frac{1}{\ln(4G/\pi\sigma)} \quad [47]$$

Although the steady-state strain rates obtained from the models developed by Weertman and Nabarro, eqns [47] and [46], respectively, differ in magnitude, these flow laws share fundamental elements. Both yield a cubic dependence of strain rate on differential stress and a linear dependence of strain rate on diffusivity. That is, both result in power-law equations similar to that given in eqn [43] with $m = 0$. The exponential dependence of strain rate on temperature enters through D as does at least part of the dependence of strain rate on

oxygen and/or water fugacity. In detail, the dependence of diffusivity on fugacity enters through the concentration of the point defects (e.g., vacancies) that enable diffusion of ions, as expressed in eqn [16].

As discussed by Hirth and Lothe (1968, pp. 506–529) and Poirier (1985, pp. 58–62), the climb velocity is directly proportional to the concentration of jogs, c_j, times the migration velocity of jogs, v_j:

$$v_c = c_j v_j \qquad [48]$$

The jog migration velocity is directly proportional to the flux of ions to or from a dislocation and thus directly proportional to the self-diffusion coefficient of the slowest ion. It is usually assumed that dislocations are fully saturated with jogs (i.e., $c_j = 1$) such that the concentration of vacancies remains at local equilibrium along the dislocation line. If the concentration of jogs is significantly below this level (i.e., $c_j << 1$), then the jog concentration introduces an extra energy term into the climb velocity, such that the activation energy for climb will be larger than that for self-diffusion of the slowest ion. In addition, as discussed below, if the jog concentration depends on the concentration of other point defects, then c_j may also be a function of thermodynamic parameters such as oxygen fugacity and water fugacity (e.g., Hobbs, 1981, 1983, 1984).

2.14.3.1.2.(ii) Grain-boundary sliding and migration Boundaries or interfaces separating neighboring grains often contribute substantially to plastic deformation of rocks. In the diffusion creep regime, sliding along grain and interphase boundaries is an essential aspect of deformation (Raj and Ashby, 1971). Thus, as discussed above, diffusion creep might be more descriptively named diffusion-accommodated grain-boundary sliding.

Grain-boundary sliding (gbs) is also important during deformation in which dislocations dominate flow. Grain-boundary sliding has received a great deal of attention in the literature on superplastic deformation, a deformation process in which a solid is deformed (in tension) to very large strains (~1000% elongation) without failing by necking and subsequent fracture (see for example, Ridley, 1995). Based on microstructural analyses, Boullier and Gueguen (1975) argued that superplastic flow is responsible for deformation in at least some mylonites. Schmid *et al.* (1977) and Goldsby and Kohlstedt (2001) discussed the possibility of superplastic flow in their deformation experiments on limestone and ice, respectively. However, as Poirier (1985, p. 204) pointed out "superplasticity is a behavior, not a definite phenomenon." Thus, in this paper, emphasis is given to the coupling between grain-boundary sliding and dislocation activity in the deformation process without appealing specifically to the term superplasticity.

In this regime, strain rate varies with differential stress according to a power-law relationship such as the one presented in eqn [43] with $n > 1$. This observation immediately implies that grain-boundary sliding cannot be accommodated simply by diffusion, which would lead to a linear dependence of strain rate on stress (e.g., Ashby and Verrall, 1973). A number of models examine deformation processes involving grain-boundary sliding coupled with dislocation motion. A few of these studies are mentioned here to bring out the key elements of this process, with more extensive lists of references available in Poirier (1985, section 7.4) and elsewhere (Kaibyshev, 1992; Langdon, 1994, 1995).

Ball and Hutchinson (1969), Mukherjee (1971), and Gifkins (1976, 1978) considered the motion of grain-boundary dislocations impeded by obstacles in the grain boundaries. Stress concentrations that develop at ledges or triple junctions are relieved by the generation of dislocations that then move through the adjoining grains. These dislocations, piled up against neighboring grain boundaries, are removed by climb into the grain boundaries. As these extrinsic dislocations move along grain boundaries, they contribute to grain-boundary sliding. Kaibyshev (2002) in particular emphasized the importance of this excess population of dislocation in the grain boundaries due to interaction of the grain boundaries with lattice dislocations. This approach leads to the flow law

$$\dot{\varepsilon} = A_{gbs} \frac{D_{gb}}{d^2} \frac{G V_m}{RT} \left(\frac{\sigma}{G}\right)^2 \qquad [49]$$

where the value of the parameter A_{gbs}, which depends on the details of the grain-boundary sliding process and the dislocation recovery mechanism (see Langdon, 1994), has a value of order 10. This type of analysis is applied to the situation in which a subgrain structure does not build up within the individual grains so that dislocations move relatively freely from one grain boundary, across the grain, to the opposite grain boundary.

If grains contain subgrains, then dislocations that are generated by sliding along a grain-boundary glide across the adjoining grain until they encounter a

subgrain boundary. The dislocations then climb into the subgrain boundary, interact with dislocations in the subgrain wall, and are annihilated (Langdon, 1994). This type of analysis leads to a flow law of the form

$$\dot{\varepsilon} = B_{\text{gbs}} \frac{D_{\text{gm}}}{d^1} \frac{GV_{\text{m}}}{RT} \left(\frac{\sigma}{G}\right)^3 \qquad [50]$$

with $B_{\text{gbs}} \approx 1000$. Note that eqns [49] and [50] differ in their dependence on stress (σ^2 vs σ^3), on grain size ($1/d^2$ vs $1/d$), and on temperature (Q_{gb} vs Q_{gm}).

In silicates, evidence for creep involving grain-boundary sliding and dislocations motion has been identified in deformation data for dry olivine (Kohlstedt and Wang, 2001; Hirth and Kohlstedt, 2003) and is apparent in the results for dry clinopyroxene (Bystricky and Mackwell, 2001) for which a coarse-grain rock is a factor of ~10 stronger than a fine-grained sample fabricated from powders prepared from the coarse-grain rock. Interestingly, this grain-boundary sliding regime appears to be absent in olivine deformed under hydrous conditions, possibly because an enhancement of dislocation climb provides the extra deformation mechanism required to fulfill the von Mises criterion (Mei *et al.*, 2002; Hirth and Kohlstedt, 2003).

In addition to their contribution to deformation by producing strain as they slide, grain boundaries facilitate deformation by migrating in response to the strain energy associated with high densities of dislocations within the grains. This dynamic recrystallization process does not itself produce strain; however, it does remove dislocations within grains, resulting in a population of small grains that are, at least initially, free of dislocations. Dislocations generated at grain boundaries can more easily glide across these dislocation-free grains, unimpeded by interactions with other dislocations, than through larger grains containing high densities of dislocations. In addition, since the contribution of grain-boundary sliding to deformation increases with decreasing grain size as indicated in eqns [49] and [50], grain-boundary sliding can contribute to deformation in regions of small grains, thus also enhancing the rate of deformation. Hence, dynamic recrystallization often results in 'strain softening', a reduction in creep strength with progressive deformation (i.e., increasing strain) of a rock (e.g., de Bresser *et al.*, 2001; Drury, 2005). Dynamic recrystallization can also occur by subgrain rotation by which dislocations are removed from the interiors of grains by addition to low-angle boundaries (e.g., Poirier, 1985, pp. 169–177). As dislocations are added to these (low-angle) subgrain boundaries, the misorientation angle increases until distinct new grains (i.e., high-angle grain boundaries) form. An example of dynamic recrystallization involving grain-boundary migration and simultaneous subgrain rotation is presented in **Figure 9**. Again, the removal of dislocations from within the grains reduces temporarily the number of obstacles to dislocation glide, and the formation of smaller grains makes the operation of grain-size-sensitive deformation processes (diffusion creep and grain-boundary sliding) more favorable.

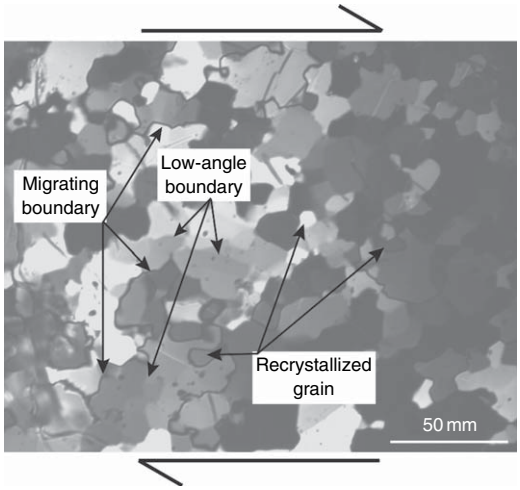

Figure 9 Transmitted-light optical micrograph with polarizers crossed of thin section of $(Fe_{0.5}Mg_{0.5})_2SiO_4$ illustrating the process of dynamic recrystallization occurring both by subgrain rotation and grain-boundary migration. Sample was deformed in torsion to a shear strain of $\gamma = 4$. Courtesy of Y-H Zhao.

2.14.3.1.2.(iii) Low-temperature plasticity At lower temperatures and hence higher stresses, power-law formulations underpredict the observed increase in strain rate with increasing stress. As temperature decreases, diffusion becomes too slow to permit a significant contribution of dislocation climb to the deformation process. The rate of deformation then becomes limited by the ability of dislocations to glide past obstacles. In silicate minerals with a significant component of covalent bonding, dislocations must overcome the resistance imposed by the lattice itself, often referred to as the Peierls barrier (e.g., Frost and Ashby, 1982, pp. 6–9). Motion of dislocations over the Peierls barrier requires the nucleation and migration of kinks (steps along dislocation lines that lie in the glide plane), with the

nucleation rate of pairs of kinks generally assumed to limit the dislocation velocity (Frost and Ashby, 1982, p. 8). The dislocation velocity is determined by the glide velocity, v_g, and consequently by the kink velocity, v_k:

$$v \approx v_g = c_k v_k \qquad [51]$$

where c_k is the concentration of kinks. The activation enthalpy for the nucleation and migration of double kinks, $\Delta H_k(\sigma)$, is a function of differential stress. A detailed analysis for $\Delta H_k(\sigma)$ yields (Kocks *et al.*, 1975, p. 243; Frost and Ashby, 1982, p. 8)

$$\Delta H_k(\sigma) = \Delta H_k^o \left[1 - \left(\frac{\sigma}{\sigma_P}\right)^r\right]^s \qquad [52]$$

where ΔH_k^o is the Helmholtz free energy of an isolated pair of kinks, σ_P is the Peierls stress, and r and s are model-dependent parameters (Frost and Ashby, 1982, p. 9). From Orowan's equation, eqn [42], the flow law then becomes

$$\dot{\varepsilon} = \dot{\varepsilon}_P \left(\frac{\sigma}{G}\right)^2 \exp - \left\{\frac{\Delta H_k^o}{RT}\left[1 - \left(\frac{\sigma}{\sigma_P}\right)^r\right]^s\right\} \qquad [53]$$

where $\dot{\varepsilon}_P$ is a material-dependent parameter.

An illustrative method for displaying the conditions under which a given deformation mechanism dominates flow is the deformation mechanism map (Frost and Ashby, 1982). At present, olivine is the only mineral for which data exist in the diffusion, dislocation, grain-boundary sliding, and low-temperature plasticity regimes. Four parameters are usually considered when constructing a deformation mechanism map: strain rate, stress, grain size, and temperature. Examination of eqn [32] indicates that other parameters could be included (e.g., pressure, water fugacity, and melt fraction) depending on the application. Here, the classical form is first used in which stress is plotted as a function of temperature for a fixed grain size (and fixed pressure, water fugacity, etc.) with strain rate shown parametrically. In **Figures 10(a)** and **10(b)**, differential stress is plotted as a function of temperature for dunite rocks composed of 10-μm grains and 1-mm grains, respectively. Flow parameters for the diffusion, dislocation, and grain-boundary sliding regimes are taken from Hirth and Kohlstedt (2003), while those for the low-temperature plasticity regime are from Goetze (1978) and Evans and Goetze (1979). For a fine-grained rock with $d = 10\,\mu m$ such as might be found in a shear zone (**Figure 10(a)**), diffusion creep dominates at geological strain rates, 10^{-15}–$10^{-10}\,s^{-1}$ for stresses below ~300 MPa. At higher stresses, grain-boundary sliding becomes important, and at still higher stresses, low-temperature plasticity dominates. For a coarser-grained rock with $d = 1\,mm$ such as might be expected in the upper mantle (**Figure 10(b)**), deformation at geological strain rates and stresses appropriate for the asthenosphere occurs near the boundary between the diffusion and dislocation creep regimes, while deformation in the lithosphere requires dislocation creep or low-temperature

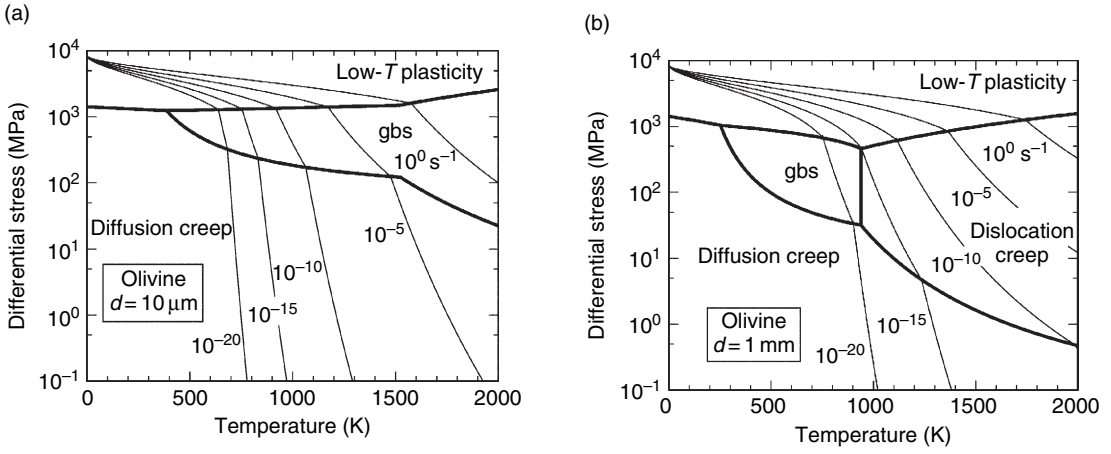

Figure 10 Deformation mechanism maps plotted as differential stress as a function of temperature for dunite with grain sizes of (a) 10 μm and (b) 1 mm. (a) At the smaller grain size for a strain rate of $10^{-15}\,s^{-1}$, deformation occurs by diffusion creep for stresses up to ~300 MPa above which deformation is dominated by grain-boundary sliding and then by low-temperature plasticity. (b) At the larger grain size for a strain rate of $10^{-15}\,s^{-1}$, with increasing stress deformation moves from the diffusion creep regime to the dislocation creep regime to the low-temperature plasticity regime.

plasticity. Strong seismic anisotropy in the mantle at depths less than ~250 km indicates that deformation occurs by dislocation processes (e.g., Montagner, 1985; Nishimura and Forsyth, 1989; Gaherty and Jordan, 1995). In contrast, the apparent lack of seismic anisotropy at greater depths, below the Lehmann discontinuity (Lehmann, 1959, 1961), has been interpreted as an indicator of diffusion creep (Karato, 1992), although more recent observations indicate that a weak anisotropy exists in this deeper region, characteristic of dislocation activity on the (*hk*0)[001] slip system (Mainprice *et al.*, 2005).

An alternative form of the deformation mechanism map that provides insight into mantle deformation process is obtained by plotting stress as a function of grain size with strain rate again shown parametrically, as illustrated in **Figure 11**. The greater importance of grain-boundary sliding at the lower temperature (800°C vs 1300°C) is clear in this comparison. This behavior reflects the fact that the activation energy for grain-boundary sliding below ~1250°C appears to be smaller than that for dislocation creep, ~400 kJ mol^{-1} versus ~500 kJ mol^{-1}(Hirth and Kohlstedt, 2003) although this point remains to be confirmed experimentally (e.g., Mei and Kohlstedt, 2000b). Also, the contribution of low-temperature plasticity is, as expected, greater at 800°C. Finally, at 1300°C for geological stresses, strain rates, and asthenospheric grain sizes, deformation occurs close to the boundary between diffusion and dislocation creep.

2.14.3.2 Role of Fluids in Rock Deformation

Two important, often-present components that can result in a substantial weakening of rocks are melt and water. If either is present, even in small concentration, it can profoundly reduce the viscosity of a rock.

2.14.3.2.1 Role of melt in rock deformation

The influence of melt on rock viscosity enters constitutive equations in two ways (Kohlstedt, 2002; Xu *et al.*, 2004). First, melt provides a path along which ions can diffuse more rapidly than they can either through grain interiors or along grain boundaries. Second, since melt does not support shear stresses, for a given applied macroscopic stress, the stress at the grain scale will be locally increased if melt is present.

Both of these contributions to the high-temperature strength of a rock were included in the analysis by Cooper *et al.* (1989) of the effect of melt on diffusion creep of an aggregate composed of a fluid plus a solid phase. Such analyses depend critically on the distribution of the melt phase. In this particular model, the melt distribution was assumed to be that dictated by surface tension for an isotropic system under a hydrostatic state of stress for which the dihedral angle, θ, is determined by the relative values

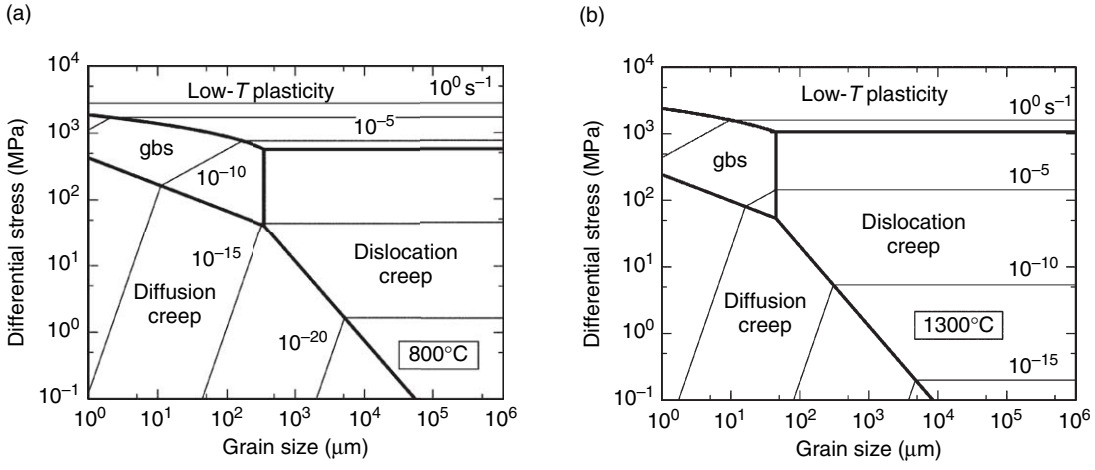

Figure 11 Deformation mechanism maps plotted as differential stress as a function of grain size for dunite at temperatures of (a) 800°C and (b) 1300°C. (a) At the lower temperature for a strain rate of 10^{-15} s^{-1}, deformation occurs by diffusion creep for grain sizes less than ~200 μm and by dislocation creep at larger grain sizes. At higher strain rates, grain-boundary sliding contributes at grain sizes smaller than ~50 μm such as might be present in shear zones. (b) At the higher temperature, deformation is dominated by diffusion creep at finer grain sizes and by dislocation creep at coarser grain sizes.

of the solid–liquid and solid–solid interfacial energies, γ_{sl} and γ_{ss}, respectively:

$$\cos\left(\frac{\theta}{2}\right) = \frac{\gamma_{ss}}{2\gamma_{sl}} \quad [54]$$

For the olivine + mid-ocean ridge basalt (MORB) case, the average dihedral angle is ~40° (i.e., $0 < \theta < 60°$) such that, ideally, melt forms an interconnected network along three-grain junctions and through four-grain corners, such as illustrated in **Figure 12**. Average values for dihedral angle of <60° are observed for many rocks composed of silicate minerals plus a silicate melt. However, as illustrated in **Figure 13**, for melt fractions greater than ~0.05 the model of Cooper and Kohlstedt (Cooper *et al.*, 1989) significantly underpredicts the decrease in viscosity measured in experiments on partially molten rocks in the diffusion creep regime (Hirth and Kohlstedt, 1995a; Zimmerman and Kohlstedt, 2004).

One important aspect not taken into account in the above analysis is the fact that the wetting behavior of most partially molten systems is not isotropic (e.g., Cooper and Kohlstedt, 1982). As illustrated in **Figure 14**, microstructural observations demonstrate that melt wets a fraction of the grain boundaries, behavior not predicted for an isotropic system with $\theta > 0°$. Furthermore, the percentage of grain boundaries wetted by melt increases with increasing melt fraction, ϕ (Hirth and Kohlstedt, 1995b). At the time of writing of this chapter, a model that appears to deal adequately with the effect of this microstructural distribution of melt on diffusion creep behavior is being developed (Takei and Holtzman, 2006). This model expresses the viscosity of a partially molten rock in terms of grain-boundary contiguity (the ratio of grain-boundary area to grain-boundary area plus grain-melt interfacial area). This model extends that of Cooper and Kohlstedt (Cooper *et al.*, 1989) from two to three dimensions and includes the observed anisotropic wetting of grains. One important result of

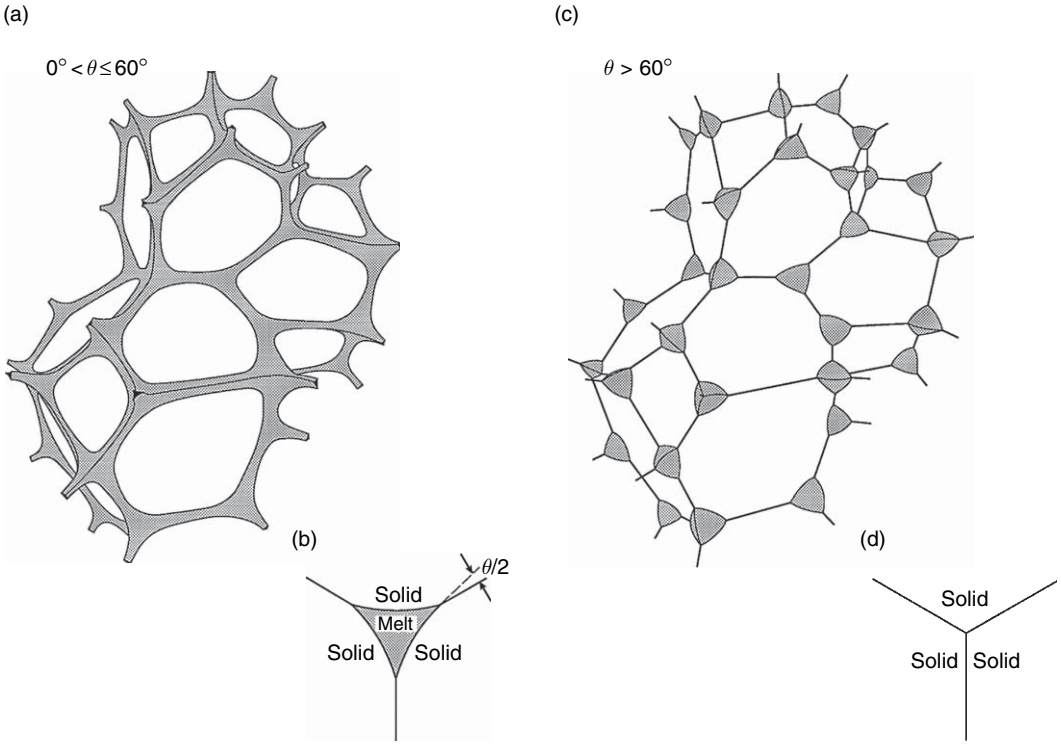

Figure 12 Sketch of melt distribution in a partially molten rock with isotropic interfacial energies. In (a) with $0° < \theta \leq 60°$, melt wets all of the triple junctions and four-grain junctions; (b) cross-section through a triple junction midway along a grain edge illustrates the presence of melt. In (c) with $\theta > 60°$, melt is confined to four-grain junctions; (d) cross-section through a triple junction midway along a grain edge illustrates the absence of melt. Adapted from Riley GN, Jr and Kohlstedt DL (1990) An experimental study of melt migration in an olivine-melt system. In: Ryan MP (ed.) *Magma Transport and Storage*, pp. 77–86. New York: John Wiley & Sons.

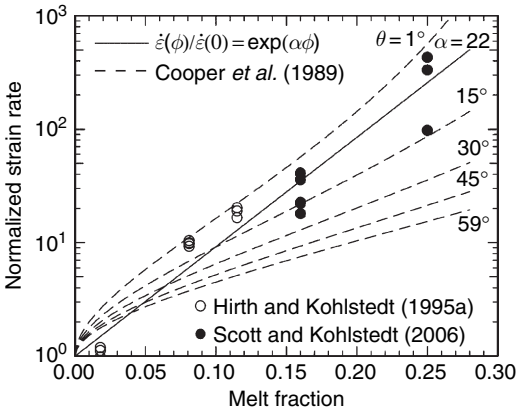

Figure 13 Plot of normalized strain rate, $\dot{\varepsilon}(\phi)/\dot{\varepsilon}(0)$, vs melt fraction. Circles are the experimentally determined values. Dashed curves are based on model of Cooper *et al.* (1989) for $1° \leq \theta \leq 59°$. Solid line is a fit of the experimental data to the empirical relationship $\dot{\varepsilon}(\phi)/\dot{\varepsilon}(0) = \exp(\alpha\phi)$, yielding $\alpha = 22$. For $\phi < 0.15$, data are from Hirth and Kohlstedt (1995a). For $\phi > 0.15$, data are from Scott and Kohlstedt (2006).

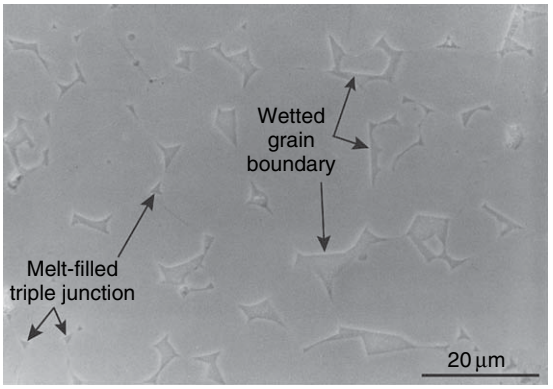

Figure 14 Backscattered scanning electron micrograph of sample of olivine +5% basalt. Both melt-filled triple junctions and wetted grain boundaries are identified. The presence of wetted grain boundaries demonstrates that the interfacial energies are anisotropic in this system, since melt would be confined to triple junctions in an isotropic system with a similar dihedral angle of $\theta \approx 40°$.

this model for the diffusion creep regime is a factor-of-five decrease in viscosity caused by increasing ϕ from 0 to 0.001 (i.e., 0.1% melt). This model yields a good fit to the experimental data for $\phi > 0$. The predicted factor-of-five decrease in viscosity in going from $\phi = 0$ to $\phi = 0.001$ has not been observed experimentally, possibly because most of the samples fabricated for these experiments contain a trace amount of melt due to impurities introduced during the crushing and grinding process or produced from inclusions within the olivine crystals used to prepare fine-grained powders from which samples were synthesized (Faul and Jackson, 2006).

Experimental determinations of strain rate as a function of melt fraction in both the diffusion creep regime and the dislocation creep regime have been empirically fit to the relation

$$\dot{\varepsilon}(\phi) = \dot{\varepsilon}(0)\exp(\alpha\phi^r) \qquad [55]$$

for melt fractions from near zero to the rheologically critical melt fraction (RCMF) with $r = 1$ for the olivine + basalt system (Kelemen *et al.*, 1997; Mei *et al.*, 2002; Scott and Kohlstedt, 2006) as well as for an organic crystal plus melt system (Takei, 2005) and $r = 3$ for a partially molten granitic rock (Rutter and Neuman, 1995, Rutter *et al.*, 2006). The RCMF is the melt fraction at which, with increasing melt fraction, viscosity of a melt-solid system moves from that of a solid framework with interstitial melt to that of a melt containing grains in suspension.

Melt has a greater effect on viscosity in the dislocation creep regime than in the diffusion creep regime, at least in the olivine + basalt and partially molten lherzolite systems (Mei *et al.*, 2002; Zimmerman and Kohlstedt, 2004; Scott and Kohlstedt, 2006). This point is illustrated in **Figure 15** with $\alpha = 21$ in the diffusion creep regime and $\alpha = 32$ in the dislocation creep regime. At melt fractions greater than the RCMF, a partially molten rock behaves as a fluid (melt) containing suspended particles. The Einstein–Roscoe equation (Roscoe, 1952),

$$\eta_{ER}(\phi) = \frac{\mu}{(1.35\phi - 0.35)^{2.5}} \qquad [56]$$

which reasonably well describes the viscosity of a system with $\phi > 0.25$–0.30, is also shown in **Figure 15**. In eqn [56], μ is melt viscosity. Finally, it should be noted that the onset of melting will affect grain-boundary chemistry, which will indirectly affect rock viscosity through its influence on the rates of ionic diffusion along grain boundaries (Hiraga *et al.*, 2007).

2.14.3.2.2 Role of water in rock deformation

Water weakening of nominally anhydrous silicate minerals was first observed in the mid-1960s in an experimental study of the strength of quartz (Griggs and Blacic, 1965). In these solid-medium deformation

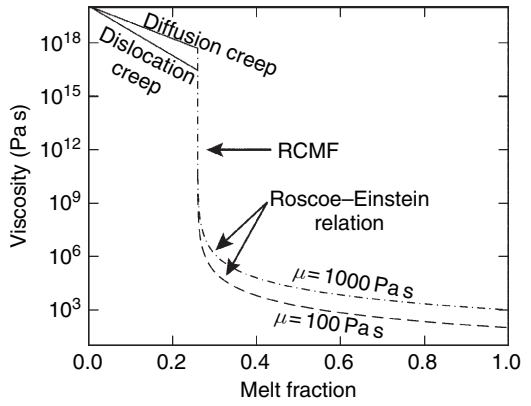

Figure 15 Plot of viscosity of a partially molten rock versus melt fraction illustrating the transition between flow controlled by a framework of solid particles with interstitial melt to flow dominated by melt with suspended particles. At low melt fractions, dislocation creep and diffusion creep are described by eqn [55] with $r = 1$ and $\alpha = 21$ and 32, respectively. At the RMCF, which marks the transition from solid-like to fluid-like behavior, viscosity plummets rapidly with increasing melt fraction. At higher melt fractions, $\phi > 0.25$–0.30, the Roscoe–Einstein relation, eqn [56], describes deformation of a mixture of melt with suspended particles. Adapted from Scott T and Kohlstedt DL (2006) The effect of large melt fraction on the deformation behavior of peridotite. *Earth and Planetary Science Letters* 246: 177–187.

experiments, samples deformed with a hydrous confining medium (talc) were weaker than samples deformed with an anhydrous confining medium. Subsequently, water weakening has been reported for other nominally anhydrous minerals (NAMs) including olivine (e.g., Avé Lallemant and Carter, 1970), pyroxene (Avé Lallemant, 1978), and feldspar (e.g., Tullis and Yund, 1980). These first studies of water weakening emphasized the phenomenon. A second generation of experiments focused on the mechanism of water weakening by studying the dependence of viscosity on water fugacity, that is, on the concentration of water-derived point defects (Kronenberg and Tullis, 1984; Kohlstedt *et al.*, 1995; Post *et al.*, 1996; Mei and Kohlstedt, 2000a, 2000b; Karato and Jung, 2003; Chen *et al.*, 2006).

The first model of water or hydrolytic weakening was built on a mechanism in which water hydrolyzes strong Si–O bonds forming weaker Si–OH···OH–Si bonds (Griggs, 1967). Thus, dislocation glide is easier under hydrous conditions than under anhydrous conditions; effectively, the Peierls stress/barrier decreases as Si–O–Si bridges become hydrolyzed. In this analysis, the rate of dislocation glide is limited by the propagation of kinks along dislocations, a process facilitated by diffusion of water along dislocation cores. The dislocation velocity is then taken to be proportional to the concentration of water (Griggs, 1974).

More recent models of water weakening have emphasized the role of water-derived point defects, particularly hydrogen ions (protons) (Hobbs, 1981, 1983, 1984; Poumellec and Jaoul, 1984; Mackwell *et al.*, 1985). Protons diffuse rapidly in NAMs (for a review, see Ingrin and Skogby, 2000) such as quartz (Kronenberg *et al.*, 1986), olivine (Mackwell and Kohlstedt, 1990; Kohlstedt and Mackwell, 1998, 1999; Demouchy and Mackwell, 2003), and pyroxene (Ingrin *et al.*, 1995; Hercule and Ingrin, 1999; Carpenter Woods *et al.*, 2000; Stalder and Skogby, 2003). Thus, initially dry, millimeter-size samples can be hydrated in high-temperature, high-pressure experiments lasting a few hours or less. The presence of protons in a NAM affects the velocity of a dislocation in two possible ways. First, since protons are charged, a change in the concentration of protons will result in a change in the concentration of all other charged point defects. Hence, the introduction of protons into a NAM will directly affect the concentrations of vacancies and self-interstitials on each ionic sublattice and consequently the rates of diffusion of the constituent ions and the rate of dislocation climb. In addition, extrinsic point defects, specifically water-derived point defects, can affect the concentrations of kinks and jogs along dislocation lines and thus dislocation velocity as expressed in eqns [48] and [51] (Hirsch, 1979, 1981; Hobbs, 1981, 1984). The effect of water-derived point defects on the concentrations of kinks and jogs can enter in two ways. First, for minerals containing a transition metal such as Fe (i.e., semiconducting silicates), the presence of water-derived point defects will affect the concentration of electron holes, $h^{\cdot}$, which in turn can affect the concentrations of kinks and jogs by ionizing initially neutral jogs (Hirsch, 1979, 1981; Hobbs, 1984). For the case of kinks, a positively charged kink, $k^{\cdot}$, can be produced from a neutral kink by the reaction

$$k^{\times} + h^{\cdot} \rightleftarrows k^{\cdot} \qquad [57]$$

for which the law of mass action yields

$$[k^{\cdot}] = K_{57}[k^{\times}][h^{\cdot}] \qquad [58]$$

The total concentration of kinks then becomes

$$[k^{tot}] = [k^{\times}] + [k^{\cdot}] = [k^{\times}](1 + K_{57}[h^{\cdot}]) \quad [59]$$

where the second term can be much larger than unity and dominate the kink population. The dependence of kink concentration on water (proton) concentration or water fugacity then enters through concentration of positively charged kinks, thus enhancing the dislocation glide velocity. A similar argument can be used for increasing the concentration of jogs, and thus the dislocation climb velocity. While this approach provides one mechanism for increasing dislocation velocity in NAMs, it is not easily extended to minerals such as quartz that do not contain significant concentrations of transition metals. Therefore, a more direct influence of water-derived point defects on kink and jog concentrations needs to be considered. In point defect notation, the addition of protons, $\dot{p}$, to a nominally anhydrous silicate will affect the concentration of kinks through a reaction such as

$$k^{\times} + \dot{p}\{k^{\times} - \dot{p}\}^{\cdot} \quad [60]$$

where the curly brackets { } indicate the formation of a neutral kink associated with a proton. Application of the law of mass action yields

$$[\{k^{\times} - \dot{p}\}^{\cdot}] = K_{60}[k^{\times}][\dot{p}] \quad [61]$$

The total concentration of kinks is then

$$[k^{tot}] = [k^{\times}] + [\{k^{\times} - \dot{p}\}^{\cdot}] = [k^{\times}](1 + K_{60}[\dot{p}]) \quad [62]$$

Again, a similar equation applies for jogs. The dependence of kink and jog concentrations on water concentration/fugacity then comes directly through the dependence of proton concentration on water fugacity.

The high-temperature deformation behaviors of anorthite, clinopyroxene, and olivine deformed in the dislocation creep regime under anhydrous and ander hydrous conditions are compared in **Figure 16**. A similar comparison is made for the diffusion creep regime by Hier-Majumder *et al.* (2005a). In the dislocation creep regime, the dependence of strain rate on water fugacity has been quantified for olivine (Mei *et al.*, 2002; Hirth and Kohlstedt, 2003; Karato and Jung, 2003) and for clinopyroxene (Chen *et al.*, 2006). In the case of olivine, strain rate increases as water fugacity to the ~1st power, while in the case of clinopyroxene, strain rate increases as water fugacity to the ~3rd power. In the diffusion creep regime, creep rate increases as water fugacity to the ~1st

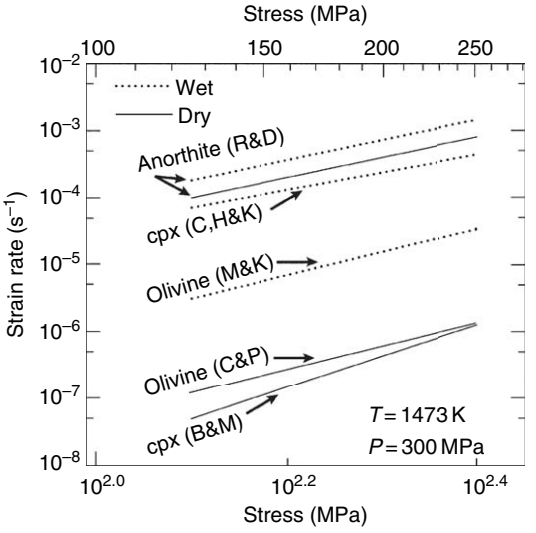

Figure 16 Strain rate vs stress for samples of anorthite, clinopyroxene, and olivine deformed in the dislocation creep regime under anhydrous and hydrous conditions. In each case, samples deformed under hydrous conditions are weaker than those deformed under anhydrous conditions. The water fugacity for samples deformed under hydrous conditions at a confining pressure of 300 MPa and 1473 K is ~300 MPa. Results are taken from R&D, Rybacki and Dresen (2000); C,H,&K, Chen *et al.* (2006); M&K, Mei and Kohlstedt (2000a); C&P, Chopra and Paterson (1984); and B&M, Bystricky and Mackwell (2001).

power for olivine (Mei and Kohlstedt, 2000a) and to the ~1.4 power for clinopyroxene (Hier-Majumder *et al.*, 2005a). To assess possible explanations for these observed dependences of strain rate on water fugacity, **Table 2** summarizes the relationships between the concentration of various point defects and water fugacity for several charge neutrality conditions for a transition-metal silicate. (1) For olivine under both anhydrous and hydrous conditions, the activation energies for dislocation creep (Hirth and Kohlstedt, 2003) and those for Si self-diffusion (Dohmen *et al.*, 2002; Chakraborty and Costa, 2004) agree within experimental error (Kohlstedt, 2006). This observation suggests that the high-temperature creep of olivine is controlled by dislocation climb limited by diffusion of the slowest ionic species, Si, under both dry and wet conditions. In this case, the jog concentration is unity, that is, the dislocations are fully saturated with jogs (see eqn [48] and the discussion that follows). Under hydrous conditions, the water fugacity exponent, q, in eqn [43] of ~1 is consistent with Si diffusing by a vacancy mechanism with the major Si vacancy being part of the point defect

Table 2 Dependence of point defect concentrations on water fugacity, expressed as the exponent q in the relationship $[\,] \propto f_{H_2O}^{q}$, for several charge neutrality conditions for a transition-metal silicate

	$[Fe_{Me}^{\cdot}]$			$[(OH)_O^{\cdot}]$								
	$[h^{\cdot}]$	$[Fe_{Si}']$	$[V_{Me}'']$	$[p^{\cdot}]$	$[H_{Me}']$	$[(2H)_{Me}^{\times}]$	$[O_i'']$	$[V_{Si}'''']$	$[H_{Si}'''']$	$[(2H)_{Si}'']$	$[(3H)_{Si}']$	$[(4H)_{Si}^{\times}]$
$[h^{\cdot}] = 2[V_{Me}'']$	0	0	0	1/2	1/2	1	0	0	1/2	1	3/2	2
$[p^{\cdot}] = 2[V_{Me}'']$	−1/6	1/6	1/3	1/3	2/3	1	1/3	2/3	1	4/3	5/3	2
$[p^{\cdot}] = [Fe_{Si}']$	−1/4	1/4	1/2	1/4	3/4	1	1/2	1	5/4	3/2	7/4	2
$[h^{\cdot}] = [H_{Me}']$	1/4	−1/4	−1/2	3/4	1/4	1	−1/2	−1	−1/4	1/2	5/4	2
$[p^{\cdot}] = [H_{Me}']$	0	0	0	1/2	1/2	1	0	0	1/2	1	3/2	2

associate $\left\{2(OH)_O^{\cdot} - V_{Si}''''\right\}'' \equiv (2H)_{Si}''$ and charge neutrality given by $\left[(OH)_O^{\cdot}\right] = [H_{Me}']$ (see **Table 2**). Diffusion of Me ions also varies as water fugacity to the 1st power (Hier-Majumder *et al.*, 2005b), indicating that $(2H)_{Me}^{\times}$ is the primary point defect on the Me sublattice responsible for diffusion (see **Table 2**). (2) The situation appears to be more complex for clinopyroxene. The stress exponent is $n = 2.7 \pm 0.3$, consistent with the climb-controlled creep models discussed above. Unfortunately, diffusion data are lacking for comparison with the creep data. The relatively strong dependence of strain rate on water fugacity, $q = 3.0 \pm 0.6$, in the dislocation creep regime suggests that a simple climb-controlled mechanism may not apply for high-temperature deformation of clinopyroxene (see **Table 2**). One possible way to reconcile this large value for the water fugacity exponent is as follows: (1) Creep is climb controlled; (2) charge neutrality condition is given by $[h^{\cdot}] = [H_{Me}']$ or by $[p^{\cdot}] = [H_{Me}']$; (3) strain rate is limited by Si diffusion by a vacancy mechanism involving the defect associate $\left\{4(OH)_O^{\cdot} - V_{Si}''''\right\}^{\times} \equiv (4H)_{Si}^{\times}$; (4) dislocations are undersaturated with jogs with the jog concentration dominated by neutral jogs associated with protons, $\left\{k^{\times} - p^{\cdot}\right\}^{\cdot}$, as in eqns [61] and [62]. These scenarios yield a water fugacity exponent for strain rate of 2¾ and 2½, both within the experimental uncertainty of the measured value. Clearly, diffusion data are critical in order to develop this type of argument more completely.

2.14.4 Upper-Mantle Viscosity

In this section, viscosity profiles for the upper mantle constrained by geophysical observations and calculated from laboratory-derived flow laws are compared. Two situations are considered: first, global average values determined from analyses of glacial isostatic adjustment are examined relative to those calculated for dunite containing $1000\,H/10^6Si$. Second, the viscosity of the upper-mantle region beneath the western US is compared to the viscosity predicted for dunite deforming under water-saturated conditions.

Laboratory results for dunite are used because it is the only rock for which data are available over a wide range of upper-mantle conditions. Justification for this choice is based on the observations that olivine is the major mineral in the upper mantle and that, under conditions for which data are available, the flow behavior of dunite is nearly identical to that of lherzolite (Zimmerman and Kohlstedt, 2004). Furthermore, flow laws for melt-free dunite are used because, at small melt fractions, homogeneously distributed melt has a relatively small effect on viscosity. For $\phi = 0.02$, viscosity is a factor of <2 smaller than the viscosity of a melt-free rock (**Figures 13** and **15**); larger melt fractions would be difficult to trap in the mantle over long periods of time. By comparison, the viscosity of dunite containing 1000 ppm water is a factor of >100 smaller than the viscosity of dry dunite (**Figure 16**). Thus, the effect of water rather than melt is emphasized here. It should be noted that melt might have a larger effect on viscosity if it segregates into melt-rich bands as observed in large-strain experiments on partially molten peridotites (Holtzman *et al.*, 2003a, 2003b, 2005); however, this area remains to be fully explored.

Finally, viscosity profiles are calculated for dislocation creep rather then diffusion creep. Three points justify this choice. First, strong seismic anisotropy at depths of <250 km (e.g., Nishimura and Forsyth, 1989) and weak but persistent seismic anisotropy at great depths (Mainprice *et al.*, 2005) indicate that deformation in the upper mantle is dominated by dislocation processes. Second, analysis of the influence of rheological properties on the evolution of the tip of a subducting slab indicates that non-Newtonian

behavior (i.e., dislocation creep) facilitates the initiation of subduction (Billen and Hirth, 2005). Third, as illustrated in **Figures 10** and **11** as well as in Hirth (2002) and Hirth and Kohlstedt (2003), deformation of dunite at temperatures above ~1000°C occurs primarily by dislocation glide and climb with contributions from grain-boundary sliding.

2.14.4.1 Upper-Mantle Viscosity Profile

Recent papers by Kaufmann and Lambeck (2002) and Hirth and Kohlstedt (2003) have investigated upper-mantle viscosity profiles based on analyses of glacial isostatic adjustment and laboratory-derived flow laws, respectively (Dixon *et al.*, 2004). Kaufmann and Lambeck (2002) examined changes of Earth's surface associated with the retreat of Late Pleistocene ice sheets to obtain global average models of viscosity profiles. They obtained a rather narrow range of values for upper-mantle viscosity of between 3×10^{20} and 3×10^{21} Pa s for the depths of 60–410 km with a best fitting result of 3×10^{20} to 5×10^{20} Pa s for 120–410 km, as illustrated in **Figure 17**, for which a rigid, elastic lithosphere overlies the viscoelastic upper mantle.

Hirth and Kohlstedt (2003) critically reviewed published experimental data from laboratory experiments on dunite rocks and olivine aggregates. Best-fit values for the flow-law parameters in eqn [43], summarized in their table 1, were used in the present analysis. The activation volume as a function of depth was calculated using their equation 3, which is based on a calculation of the elastic strain necessary to create and move point defects. The temperature as a function of depth was determined based on an adiabatic geotherm with a potential temperature, T_p, of 1350°C. A water concentration of 1000 H/10^6Si was employed following the study of Hirth and Kohlstedt (1996). Two viscosity profiles are presented in **Figure 17**, one assuming constant stress (σ = constant) and the other assuming constant rate of viscous energy dissipation, that is, $\sigma\dot{\varepsilon}$ = constant (e.g., Christensen, 1989). For additional details, the reader is referred to Hirth and Kohlstedt (2003). The viscosity profile with $\sigma\dot{\varepsilon}$ constant, which changes by a factor of three in viscosity in going from 60 to 410 km, is much steeper than the viscosity profile with σ constant, which changes by a factor of 120 in viscosity over the same depth range. Hence, it is difficult to reconcile profiles obtained with σ constant with the constraints obtained from glacial isostatic adjustment results. In contrast, profiles produced from laboratory data with $\sigma\dot{\varepsilon}$ constant are in reasonably good agreement in terms of both the narrow width and the magnitude reported from the glacial isostatic adjustment analyses.

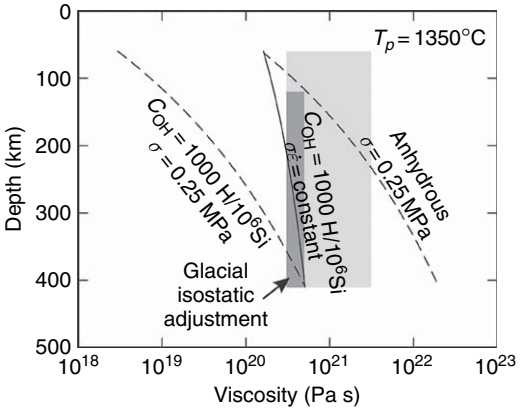

Figure 17 Viscosity profiles for anhydrous dunite with σ = 0.25 MPa, for hydrous dunite with C_{OH} = 1000 H/10^6Si with σ = 0.25 MPa, and for hydrous dunite with C_{OH} = 1000 H/10^6Si with $\sigma\dot{\varepsilon}$ = constant. Flow-law parameters are from Hirth and Kohlstedt (2003). The light gray box defines the range of global average values reported by Kaufmann and Lambeck (2002) based on analyses of glacial isostatic adjustment. The dark gray box delineates the range of global average values reported by Kaufmann and Lambeck (2002) for their best-fitting result from analyses of glacial isostatic adjustment.

2.14.4.2 Western US Mantle Viscosity Profile

In their analysis of the role of water on the lateral variation in upper-mantle viscosity, Dixon *et al.* (2004) tabulated constraints on the viscosity structure of the upper mantle beneath the western US (their table 1). Values of viscosity were based on the investigations of Bills *et al.* (1994), Kaufmann and Amelung (2000), Nishimura and Thatcher (2003), and Pollitz *et al.* (2000, 2003). These studies examined the response of Earth's surface to smaller, more local loads (earthquakes and lake level changes) than analyzed in the glacial isostatic adjustment work. Thus, their resolution is best in the shallower portion of the upper mantle. Dixon *et al.* (2004) emphasized the distinctly lower values of mantle viscosity observed in the western US (10^{18}–10^{19} Pa s) compared with the global average values (10^{20}–10^{21} Pa s). These authors make a compelling case that this difference is due to enrichment in water of the upper mantle beneath the western US associated with subduction of the Farallon Plate, which hydrates and weakens the mantle. In **Figure 18**, the range of viscosity obtained for

the western US is compared with viscosity profiles calculated based on the flow laws determined by Hirth and Kohlstedt (2003). Viscosity profiles are again calculated for σ constant and for $\sigma\dot{\varepsilon}$ constant. The geotherm was taken from figure 1 of Dixon *et al.* (2004), which was obtained from P-wave tomographic inversion for the western US (Goes and van der Lee, 2002). Water content was taken to be saturated following the solubility law determined by Kohlstedt *et al.* (1996) and Zhao *et al.* (2004). As illustrated in **Figure 18**, the flow law for dislocation creep of dunite determined from laboratory experiments yields a viscosity profile that falls within the range of values obtained from measurements of Earth's response to changes in more local surface loads. The profile with $\sigma\dot{\varepsilon}$ constant yields a relatively small decrease in viscosity with increasing depth, while the profile with σ constant produces a much larger decrease in viscosity over the same depth range. In either case, the good agreement between the viscosity profiles determined from field observation and those calculated based on experimentally determined flow laws supports extrapolation of the laboratory-derived constitutive equations to problems of geophysical interest.

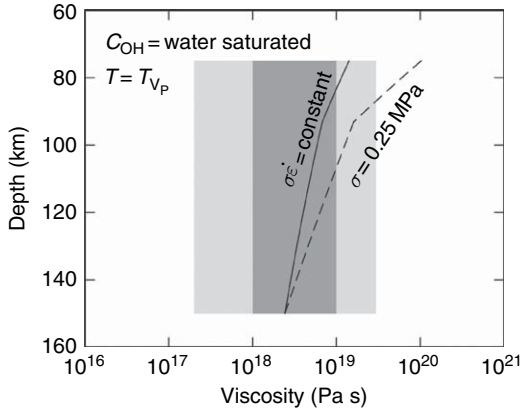

Figure 18 Viscosity profiles for water-saturated dunite with $\sigma = 0.25$ MPa and with $\sigma\dot{\varepsilon} =$ constant using flow-law parameters from Hirth and Kohlstedt (2003). Temperature profile is taken from figure 1 of Dixon *et al.* (2004), which comes from the P-wave tomography inversion of Goes and van der Lee (2002). Water concentration was taken to be saturated and was determined from the studies of Kohlstedt *et al.* (1996) and Zhao *et al.* (2004). The light gray box delineates the range of values summarized by Dixon *et al.* (2004) for the western US based on the work of Bills *et al.* (1994), Kaufmann and Ameluing (2000), Nishimura and Thatcher (2003), Politz *et al.* (2000), and Politz (2003). The dark gray box defines the viscosity bounds at 10^{18}–10^{19} Pa s.

2.14.5 Concluding Remarks

While the good agreement between laboratory and field observations for the viscosity structure of the upper mantle is encouraging, even exciting, several important areas remain that require experimental investigation of the rheological properties of mantle rocks. Possibly the most obvious void is the paucity of deformation studies on transition zone and lower-mantle minerals and rocks. Progress in this field has been slow, largely due to a lack of apparatuses capable of carrying out experiments under well-controlled thermomechanical conditions at very high pressures. However, recent developments combining a new generation of deformation apparatuses such as the deformation DIA (D-DIA) and the rotational Drickamer apparatus (RDA) with high-intensity, synchrotron-produced X-rays hold promise for significant progress in this area (e.g., Durham *et al.*, 2002; Thurel *et al.*, 2003; Xu *et al.*, 2003, 2005).

For the upper mantle, further work is needed to quantify the deformation behavior in the low-temperature plasticity regime, particularly under hydrous conditions, for application to studies of deformation of the lithosphere. Furthermore, laboratory (e.g., Jung and Karato, 2001) and seismic (e.g., Mainprice *et al.*, 2005) observations indicate that a transition in slip system occurs below a depth of ~250 km in Earth's upper mantle, related to changes in water, stress, and/or pressure conditions. At present, flow laws for the upper mantle are primarily based on experiments carried out at relatively modest pressures for which measurements of lattice-preferred orientations indicate that deformation in olivine is dominated by dislocations with [100] Burgers vectors. If dislocations with [001] Burgers vectors become important in deeper portions of the upper mantle, the flow law determined at very high pressures may deviate from that extrapolated from lower pressure conditions (Couvy *et al.*, 2004).

Finally, to date, most studies of plastic deformation of rocks have concentrated on steady-state creep with little attention given to transient deformation. While a steady-state approach may work reasonably well for describing convective flow in the mantle, it cannot provide an adequate description of deformation that occurs in an environment for which thermomechanical conditions are changing and microstructures are simultaneously evolving (e.g., Evans, 2005). This point has been appreciated by a number of researchers, some of whom have taken

a state-variable or mechanical-equation-of-state approach (e.g., Lerner and Kohlstedt, 1981; Covey-Crump, 1994, 1998; Rutter, 1999; Stone *et al.*, 2004). Such approaches will be critical in the development of the next generation of constitutive equations, which must be capable of describing flow in regions such as shear zones and metamorphic belts where changes in thermal and chemical environment including fluid chemistry and evolution of materials parameters including dislocation density, grain size, and lattice-preferred orientation occur continuously.

Acknowledgments

This work was supported by NSF grants OCE-0327143 and 0648020 (deformation of partially molten rocks), EAR- 0439747 (deformation of nominally anhydrous minerals), and EAR-0409719 (grain boundaries in rocks).

References

Ashby MF and Verrall RA (1973) Micromechanisms of flow and fracture and their relevance to the rheology of the upper mantle. *Philosophical Transactions of the Royal Society of London* A 288: 59–95.

Atkinson A (1985) Grain boundary diffusion – Structural effects and mechanisms. *Journal de Physique* 46: 379–391.

Avé Lallemant HG (1978) Experimental deformation of diopside and websterite. *Tectonophysics* 48: 1–27.

Avé Lallemant HG and Carter NL (1970) Syntectonic recrystallization of olivine and modes of flow in the upper mantle. *Geological Society of American Bulletin* 81: 2203–2220.

Ball A and Hutchinson MM (1969) Superplasticity in the aluminium–zinc eutectoid. *Metal Science Journal* 3: 1–7.

Bardeen J and Herring C (1952) Diffusion in alloys and the Kirkendall effect. In: Shockley (ed.) *Imperfections in Nearly Perfect Crystals*, pp. 261–288. New York: Wiley.

Billen MI and Hirth G (2005) Newtonian versus non-Newtonian upper mantle viscosity: Implications for subduction initiation. *Geophysical Research Letters* 32: L19304 (doi:10.1029/2005GL023457).

Bills BG, Currey DR, and Marshall GA (1994) Viscosity estimates for the crust and upper mantle from patterns of lacustrine shoreline deformation in the eastern Great Basin. *Journal of Geophysical Research* 99: 22059–22096.

Boullier AM and Gueguen Y (1975) Origin of some mylonites by superplastic flow. *Contributions to Mineralogy and Petrology* 50: 93–104.

Bystricky M and Mackwell SJ (2001) Creep of dry clinopyroxene aggregates. *Journal of Geophysical Research* 106: 13443–13454.

Cannon WR and Langdon TG (1988) Review: Creep of ceramics. Part 2: An examination of flow mechanism. *Journal of Materials Science* 23: 1–20.

Carpenter Woods S, Mackwell SJ, and Dyar D (2000) Hydrogen in diopside: Diffusion profiles. *The American Mineralogist* 85: 480–487.

Carter CB and Sass SL (1981) Electron diffraction and microscopy techniques for studying grain boundary structure. *Journal of the American Ceramic Society* 64(6): 335–345.

Carter NL and Avé Lallemant HG (1970) High temperature deformation of dunite and peridotite. *Bulletin of the Geological Society of America* 81: 2181–2202.

Catlow CRA, Bell RG, and Gale JD (1994) Computer modeling as a technique in materials chemistry. *Journal of Materials Chemistry* 4: 781–792 (doi:10.1039/JM9940400781).

Chakraborty S and Costa F (2004) Fast diffusion of Si and O in San Carlos olivine under hydrous conditions. *Goldschmidt Conference*, Copenhagen, Denmark.

Chan S-W and Balluffi RW (1985) Study of energy vs. misorientation for grain boundaries in gold by crystallite rotation method. I: (001) Twist boundaries. *Acta Metallurgica* 33: 1113–1119.

Chan S-W and Balluffi RW (1986) Study of energy vs. misorientation for grain boundaries in gold by crystallite rotation method. Part II: Tilt boundaries and mixed boundaries. *Acta Metallurgica* 34: 2191–2199.

Chen S, Hiraga T, and Kohlstedt DL (2006) Water weakening of clinopyroxene in the dislocation creep regime. *Journal of Geophysical Research* 111: B08203 (doi:10.1029/2005JB003885).

Chopra PN and Paterson MS (1984) The role of water in the deformation of dunite. *Journal of Geophysical Research* 89: 7681–7876.

Christensen UR (1989) Mantle rheology, constitution, and convection. In: Peltier WR (ed.) *Mantle Convection: Plate Tectonics and Global Dynamics, The Fluid Mechanics of Astrophysics and Geophysics*, pp. 595–655. New York: Gordon and Breach Science Publishers.

Coble R (1963) A model for boundary diffusion controlled creep in polycrystalline materials. *Journal of Applied Physics* 34: 1679–1682.

Cooper RF and Kohlstedt DL (1982) Interfacial energies in the olivine-basalt system. In: Akimota S and Manghnani MH (eds.) *High-Pressure Research in Geophysics, Advances in Earth and Planetary Sciences*, vol. 12, pp. 217–228. Tokyo: Center for Academic Publications Japan.

Cooper RF, Kohlstedt DL, and Chyung K (1989) Solution-precipitation enhanced creep in solid–liquid aggregates which display a non-zero dihedral angle. *Acta Metallurgica* 37: 1759–1771.

Couvy H, Frost D, Heidelbach F, *et al.* (2004) Shear deformation experiments of forsterite at 11 GPa – 1400°C in the multianvil apparatus. *European Journal of Mineralogy* 16: 877–889.

Covey-Crump SJ (1994) The application of Hart's state variable description of inelastic deformation to Carrara marble at $T < 450$°C. *Journal of Geophysical Research* 99: 19793–19808.

Covey-Crump SJ (1998) Evolution of mechanical state in Carrara marble during deformation at 400°C to 700°C. *Journal of Geophysical Research* 103: 29781–29794.

de Bresser JHP, Ter Heege JH, and Spiers CJ (2001) Grain size reduction by dynamic recrystallization: Can it result in major rheological weakening? *International Journal of Earth Sciences* 90: 28–45.

Demouchy S and Mackwell SJ (2003) Water diffusion in synthetic iron-free forsterite. *Physics and Chemistry of Minerals* 30: 486–494 (doi: 10.1007/s00269-003-0342-2).

Devereux OF (1983) *Topics in Metallurgical Thermodynamics*, 494pp. New York: Wiley.

Dimos D, Wolfenstine J, and Kohlstedt DL (1988) Kinetic demixing and decomposition of multicomponent oxides due to a nonhydrostatic stress. *Acta Metallurgica* 36: 1543–1552.

Dixon JE, Dixon TH, Bell DR, and Malservisi R (2004) Lateral variation in upper mantle viscosity: Role of water. *Earth and Planetary Science Letters* 222: 451–467.

Dohmen R, Chakraborty S, and Becker H-W (2002) Si and O diffusion in olivine and implications for characterizing plastic flow in the mantle. *Journal of Geophysical Research* 29: 2030 (doi:10.1029/2002GL015480).

Dorn JE (1956) Some fundamental experiments on high temperature creep. In: *Creep and Fracture of Metals at High Temperatures*, pp. 89–132. London: Her Majesty's Stationary Office.

Drury MR (2005) Dynamic recrystallization and strain softening of olivine aggregates in the laboratory and the lithosphere. In: Gapais D, Brun JP, and Cobbold PR (eds.) Geological Society, Special Publications: *Deformation Mechanisms, Rheology and Tectonics: From Minerals to the Lithosphere,* vol. 243, pp. 143–158. London: Geological Society.

Durham WB, Weidner DJ, Karato S-I, and Wang Y (2002) New developments in deformation experiments at high pressure (review). In: Karato S-I and Wenk H-R (eds.) *Plastic Deformation of Minerals and Rocks, Reviews in Mineralogy*, vol. 5, pp. 21–49. Washington DC: Mineralogical Society of America.

Evans B (2005) Creep constitutive laws for rocks with evolving structure. In: Bruhn D and Burlini L (eds.) *Geophysical Society, Speical Publications: High Strain Zones: Structure and Physical Properties,* vol. 245, pp. 329–346. London: Geological Society.

Evans B and Goetze C (1979) The temperature variation of hardness of olivine and its implications for polycrystalline yield stress. *Journal of Geophysical Research* 84: 5505–5524.

Evans B and Kohlstedt DL (1995) Rheology of rocks. In: Ahrens (ed.) *Rock Physics and Phase Relations: A Handbook of Physical Constants*, pp. 48–165. Washington: American Geophysical Union.

Evans HE and Knowles G (1978) Dislocation creep in non-metallic materials. *Acta Metallurgica* 26: 141–145.

Faul U and Jackson I (2006) The effect of melt on the creep strength of polycrystalline olivine. *EOS Transactions of the American Geophysical Union.* Fall Meeting Supplement 87(52): MR11B-0129.

Frank FC and Read WT (1950) Multiplication processes for slow moving dislocations. *Physical Review* 70: 722–723.

Frost HJ and Ashby MF (1982) *Deformation-Mechanism Maps: The Plasticity and Creep of Metals and Ceramics*, 166pp. Oxford: Pergamon Press.

Gaherty JB and Jordan TH (1995) Lehmann discontinuity at the base of an anisotropic layer beneath continents. *Science* 268: 1468–1471.

Gifkins RC (1976) Grain boundary sliding and its accommodation during creep and superplasticity. *Metallurgical Transactions* 7A: 1225–1232.

Gifkins RC (1978) Grain rearrangements during superplastic deformation. *Journal of Material Science* 13: 1924–1936.

Goes S and van der Lee S (2002) Thermal structure of the North American uppermost mantle inferred from seismic tomography. *Journal of Geophysical Research* 107 (doi:10.1029/2000JB000049).

Goetze C (1978) The mechanisms of creep in olivine. *Philosophical Transactions of the Royal Society of London A* 288: 99–119.

Goetze C and Kohlstedt DL (1973) Laboratory study of dislocation climb and diffusion in olivine. *Journal of Geophysical Research* 78: 5961–5971.

Goldsby DL and Kohlstedt DL (2001) Superplastic deformation of ice: Experimental observations. *Journal of Geophysical Research* 106: 11017–11030.

Gordon RS (1973) Mass transport in the diffusional creep of ionic solids. *Journal of the American Ceramic Society* 56: 147–152.

Griggs DT (1967) Hydrolytic weakening of quartz and other silicates. *Geophysical Journal of the Royal Astronomical Society* 14: 19–31.

Griggs DT (1974) A model of hydrolytic weakening in quartz. *Journal of Geophysical Research* 79: 1653–1661.

Griggs DT and Blacic JD (1965) Quartz: Anomalous weakness of synthetic crystals. *Science* 147: 292–295.

Groves GW and Kelly A (1969) Change of shape due to dislocation climb. *Philosophical Magazine* 19: 977–986.

Hercule S and Ingrin J (1999) Hydrogen in diopside: Diffusion, kinetics of extraction-incorporation, and solubility. *The American Mineralogist* 84: 1577–1587.

Herring C (1950) Diffusional viscosity of a polycrystalline solid. *Journal of Applied Physics* 21: 437–445.

Hier-Majumder S, Anderson IM, and Kohlstedt DL (2005b) Influence of protons on Fe–Mg interdiffusion in olivine. *Journal of Geophysical Research* 110: B02202 (doi:10.1029/2004JB003292).

Hier-Majumder S, Mei S, and Kohlstedt DL (2005a) Water weakening in clinopyroxene in diffusion creep. *Journal of Geophysical Research* 110: B07406 (doi:10.1029/2004JB003414).

Hilbrandt N and Martin M (1998) High-temperature point defect equilibria in iron-doped MgO: An *in situ* Fe-K XAFS study on the valence and site distribution of iron in $(Mg_{1-x}Fex)O$. *Berichte der Bunsengesellschaft fuer Physikalische Chemie* 102: 1747–1759.

Hiraga T, Anderson IM, and Kohlstedt DL (2003) Chemistry of grain boundaries in mantle rocks. *The American Mineralogist* 88: 1015–1019.

Hiraga T, Anderson IM, and Kohlstedt DL (2004) Partitioning in mantle rocks: Grain boundaries as reservoirs of incompatible elements. *Nature* 427: 699–703.

Hiraga T, Hirschmann MM, and Kohlstedt DL (2007) Equilibrium interface segregation in the diopside–forsterite system. II: Applications of interface enrichment to mantle geochemistry. *Geochimica et Cosmochimica Acta* 71: 1281–1289 (doi:10.1016/j.gca.2006.11.020).

Hiraga T and Kohlstedt DL (2007) Equilibrium interface segregation in the diopside-forsterite system. I: Analytical techniques, thermodynamics, and segregation characteristics. *Geochimica et Cosmochimica Acta* 71: 266–280 (doi:10.1016/j.gca.2006.11.019).

Hirsch PB (1979) A mechanism for the effect of doping on dislocation mobility. *Journal de Physique* 40(C6): 117–121.

Hirsch PB (1981) Plastic deformation and electronic mechanisms in semiconductors and insulators. *Journal of Physical Colloquium* 42(C3): 149–159.

Hirth G (2002) Laboratory constraints on the rheology of the upper mantle. In: Karato S-I and Wenk H-R (eds.) *Plastic Deformation in Minerals and Rocks, Reviews in Mineralogy and Geochemistry*, vol. 51, pp. 97–120. Washington, DC: Mineralogical Society of America.

Hirth G and Kohlstedt DL (1995a) Experimental constraints on the dynamics of the partially molten upper mantle. Deformation in the diffusion creep regime. *Journal of Geophysical Research* 100: 1981–2001.

Hirth G and Kohlstedt DL (1995b) Experimental constraints on the dynamics of the partially molten upper mantle. 2: Deformation in the dislocation creep regime. *Journal of Geophysical Research* 100: 15441–15449.

Hirth G and Kohlstedt DL (1996) Water in the oceanic upper mantle: Implications for rheology, melt extraction and the evolution of the lithosphere. *Earth and Planetary Science Letters* 144: 93–108.

Hirth G and Kohlstedt DL (2003) Rheology of the upper mantle and the mantle wedge: A view from the experimentalists. In: Eiler J (ed.) *Geophysical Monograph, Vol.138: Inside the*

Subduction Factory, pp. 83–105. Washington, DC: American Geophysical Union.

Hirth JP and Lothe J (1968) *Theory of Dislocations*, 780pp. New York: McGraw-Hill Book Company.

Hobbs BE (1981) The influence of metamorphic environment upon the deformation of materials. *Tectonophysics* 78: 335–383.

Hobbs BE (1983) Constraints on the mechanism of deformation of olivine imposed by defect chemistry. *Tectonophysics* 78: 335–383.

Hobbs BE (1984) Point defect chemistry of minerals under hydrothermal environment. *Journal of Geophysical Research* 89: 4026–4038.

Holtzman BK, Groebner NH, Zimmerman ME, Ginsberg SB, and Kohlstedt DL (2003a) Deformation-driven melt segregation in partially molten rocks. *Geochemistry Geophysics Geosystems* 4: 8607 (doi:10.1029/2001GC000258).

Holtzman BK, Kohlstedt DL, and Phipps Morgan J (2005) Viscous energy dissipation and strain partitioning in partially molten rocks. *Journal of Petrology* 46: 2569–2592 (doi:10.1093/petrology/egi065).

Holtzman BK, Kohlstedt DL, Zimmerman ME, Heidelbach F, Hiraga T, and Hustoft J (2003b) Melt segregation and strain partitioning: Implications for seismic anisotropy and mantle flow. *Science* 301: 1227–1230.

Hutchinson JW (1976) Bounds and self-consistent estimates for creep of polycrystalline materials. *Proceedings of the Royal Society of London* A 348: 101–127.

Ingrin J, Hercule S, and Charton T (1995) Diffusion of hydrogen in diopside: Results of dehydration experiments. *Journal of Geophysical Research* 100: 15489–15499.

Ingrin J and Skogby H (2000) Hydrogen in nominally anhydrous upper-mantle minerals: Concentration levels and implications. *European Journal of Mineralogy* 12: 543–570.

Jaoul O (1990) Multicomponent diffusion and creep in olivine. *Journal of Geophysical Research* 95: 17631–17642.

Jung H and Karato S-I (2001) Water-induced fabric transitions in olivine. *Science* 293: 1460–1463.

Kaibyshev O (1992) *Superplasticity of Alloys, Intermetallides, and Ceramics*. Berlin/New York: Springer.

Kaibyshev OA (2002) Fundamental aspects of superplastic deformation. *Materials Science and Engineering* 324: 96–102.

Karato S-I (1992) On the Lehmann discontinuity. *Geophysical Research Letters* 19: 2255–2258.

Karato S-I and Jung H (2003) Effects of pressure on high-temperature dislocation creep in olivine. *Philosophical Magazine* 83: 401–414.

Kaufmann G and Amelung F (2000) Reservoir-induced deformation and continental rheology in vicinity of Lake Mead, Nevada. *Journal of Geophysical Research* 105: 16341–16358.

Kaufmann G and Lambeck K (2002) Glacial isostatic adjustment and the radial viscosity profile from inverse modeling. *Journal of Geophysical Research* 107: 2280 (doi:10.1029/2001JB000941).

Kelemen PB, Hirth G, Shimizu N, Spiegelman M, and Dick HJB (1997) A review of melt migration processes in the adiabatically upwelling mantle beneath spreading ridges. *Philosophical Transactions of the Royal Society of London A* 355: 283–318.

Kelly A and Groves GW (1969) Change in shape due to dislocation climb. *Philosophical Magazine* 19: 977–986.

Kelly A and Groves GW (1970) *Crystallography and Crystal Defects*, 428pp. Reading, MA: Addison-Wesley Publishing Company.

Kocks UF, Argon AS, and Ashby MF (1975) Thermodynamics and kinetics of slip. In: *Progress in Materials Sciences*, vol. 19, 288pp. New York: Pergamon Press.

Kohlstedt DL (1992) Structure, rheology and permeability of partially molten rocks at low melt fractions. In: Phipps-Morgan J, Blackman DK, and Sinton JM (eds.) *Geophysical Monographs, Vol 71: Mantle Flow and Melt Generation at Mid-Ocean Ridges,* pp. 103–121. Washington: American Geophysical Union.

Kohlstedt DL (2002) Partial melting and deformation. In: Karato S-I and Wenk HR (eds.) *Plastic Deformation in Minerals and Rocks*, *Reviews in Mineralogy and Geochemistry*, vol. 51, pp. 105–125. Washington, DC: Mineralogical Society of America.

Kohlstedt DL (2006) The role of water in high-temperature rock deformation. In: Keppler H and Smyth J (eds.) *Water in Nominally Anhydrous Minerals, Reviews in Mineralogy and Geochemistry*, vol. 62, pp. 377–396. Washington, DC: Mineralogical Society of America.

Kohlstedt DL, Evans B, and Mackwell SJ (1995) Strength of the lithosphere: Constraints imposed by laboratory experiments. *Journal of Geophysical Research* 100: 17587–17602.

Kohlstedt DL, Keppler H, and Rubie DC (1996) Solubility of water in the α, β and γ phases of $(Mg,Fe)_2SiO_4$. *Contributions to Mineralogy and Petrology* 123: 345–357.

Kohlstedt DL and Mackwell SJ (1998) Diffusion of hydrogen and intrinsic point defects in olivine. *Zeitschrift fur Physikalische Chemie* 207: 147–162.

Kohlstedt DL and Mackwell SJ (1999) Solubility and diffusion of 'water' in silicate minerals. In: Wright K and Catlow R (eds.) *Microscopic Properties and Processes in Minerals*, pp. 539–559. Netherlands: Kluwer Academic Publishers.

Kohlstedt DL and Wang Z (2001) Grain-boundary sliding accommodated dislocation creep in dunite. Fall Meeting Supplement Abstract 82(47): T21C-01.

Kröger FA and Vink HJ (1956) Relation between the concentrations of imperfections in crystalline solids. In: Seitz F and Turnball D (eds.) *Solid State Physics*, vol. 3, pp. 307–435. San Diego CA: Academic Press.

Kronenberg AK, Kirby SH, Aines RD, and Rossman GR (1986) Solubility and diffusional uptake of hydrogen in quartz at high water pressures: Implications for hydrolytic weakening. *Journal of Geophysical Research* 91: 12723–12744.

Kronenberg AK and Tullis J (1984) Flow strengths of quartz aggregates: Grain size and pressure effects due to hydrolytic weakening. *Journal of Geophysical Research* 89: 4281–4297.

Langdon TG (1994) A unified approach to grain boundary sliding in creep and superplasticity. *Acta Metallurgica et Materialia* 42: 2437–2443.

Langdon TG (1995) Mechanisms of superplastic flow. In: Ridley N (ed.) *Superplasticity: 60 Years after Pearson*, pp. 9–24. London: Institute of Materials.

Lehmann I (1959) Velocities of longitudinal waves in the upper part of the Earth's mantle. *Annales de Geophysique* 15: 93–118.

Lehmann I (1961) S and the structure of the upper mantle. *Geophysical Journal of the Royal Astronomical Society* 4: 124–138.

Lerner I and Kohlstedt DL (1981) Effect of γ radiation on plastic flow of NaCl. *Journal of the American Ceramic Society* 64: 105–108.

Liftshitz IM (1963) On the theory of diffusion-viscous flow of polycrystalline bodies. *Soviet Physics JETP* 17: 909–920.

Mackwell SJ, Dimos D, and Kohlstedt DL (1988) Transient creep of olivine: Point defect relaxation times. *Philosophical Magazine A* 57: 779–789.

Mackwell SJ and Kohlstedt DL (1990) Diffusion of hydrogen in olivine: Implications for water in the mantle. *Journal of Geophysical Research* 95: 5079–5088.

Mackwell SJ, Kohlstedt DL, and Paterson MS (1985) The role of water in the deformation of olivine single crystals. *Journal of Geophysical Research* 90: 11319–11333.

Mainprice D, Tommasi A, Couvy H, Cordier P, and Frost DJ (2005) Pressure sensitivity of olivine slip systems and seismic anisotropy of Earth's upper mantle. *Nature* 433: 731–733.

Mei S, Bai W, Hiraga T, and Kohlstedt DL (2002) Influence of water on plastic deformation of olivine–basalt aggregates. *Earth and Planetary Science Letters* 201: 491–507.

Mei S and Kohlstedt DL (2000a) Influence of water on plastic deformation of olivine aggregates. Part 2: Dislocation creep regime. *Journal of Geophysical Research* 105: 21471–21481.

Mei S and Kohlstedt DL (2000b) Influence of water on plastic deformation of olivine aggregates. 1: Diffusion creep regime. *Journal of Geophysical Research* 105: 21457–21469.

Mishin Y and Herzig C (1999) Grain boundary diffusion: Recent progress and future research. *Materials Science and Engineering* A260: 55–71.

Montagner J-P (1985) Seismic anisotropy of the Pacific Ocean inferred from long-period surface waves dispersion. *Physics of the Earth and Planetary Interiors* 38: 28–50.

Mott NF (1951) The mechanical properties of metals. *Proceedings of the Physical Society* 64: 729–742.

Mott NF (1953) A theory of work hardening of metals. II: Flow without slip lines, recovery and creep. *Philosophical Magazine* 44: 742.

Mott NF (1956) A discussion of some models of the rate-determining process in creep. In: *Creep and Fracture of Metals at High Temperatures*, pp. 21–24. London: Her Majesty's Stationary Office.

Mukherjee AK (1971) The rate controlling mechanism in superplasticity. *Materials Science and Engineering* 8: 83–89.

Mukerjee AK, Bird JE, and Dorn JE (1969) Experimental correlations for high-temperature creep. *Transactions of ASME* 62: 155–179.

Nabarro F (1948) Deformation of crystals by the motion of single ions. In: *Report on a Conference on the Strength of Solids*, pp. 75–90. London: Physical Society.

Nabarro FRN (1967) Steady-state diffusional creep. *Philosophical Magazine* 16: 231–237.

Nakamura A and Schmalzried H (1983) On the nonstoichiometry and point defects of olivine. *Physics and Chemistry of Minerals* 10: 27–37.

Nakamura A and Schmalzried H (1984) On the Fe^{2+}–Mg^{2+} interdiffusion in olivine. *Berichte der Bunsengesellschaft fuer Physikalische Chemie* 88: 140–145.

Nishimura CE and Forsyth DW (1989) The anisotropic structure of the upper mantle in the Pacific. *Geophysical Journal* 96: 203–230.

Nishimura T and Thatcher W (2003) Rheology of the lithosphere inferred from post-seismic uplift following the 1959 Hebgen Lake earthquake. *Journal of Geophysical Research* 108: 2389 (doi:10.1029/2002JB002191).

Nix WD, Gasca-Neri R, and Hirth JP (1971) A contribution to the theory of dislocation climb. *Philosophical Magazine* 23: 1339–1349.

Orowan E (1940) Problems of plastic gliding. *Proceedings of the Physical Society* 52: 8–22.

Paterson MS (1969) The ductility of rocks. In: Argon AS (ed.) *Physics of Strength and Plasticity*, pp. 377–392. Cambridge, MA: MIT Press.

Peach MO and Koehler JS (1950) The forces exerted on dislocations and the stress fields produced by them. *Physical Review* 80: 436–439.

Poirier JP (1985) *Creep of Crystals: High-temperature Deformation Processes in Metals, Ceramics and Minerals*, 260pp. Cambridge: Cambridge University Press.

Pollitz FF (2003) Transient rheology of the uppermost mantle beneath the Mojave Desert, California. *Earth and Planetary Science Letters* 215: 89–104.

Pollitz FF, Peltzer G, and Bürgmann R (2000) Mobility of continental mantle; evidence from postseismic geodetic observations following the 1992 Landers earthquake. *Journal of Geophysical Research* 105: 8035–8054.

Post AD, Tullis J, and Yund RA (1996) Effects of chemical environment on dislocation creep of quartzite. *Journal of Geophysical Research* 101: 22143–22155.

Poumellec B and Jaoul O (1984) Influence of pO_2 and pH_2O on the high temperature plasticity of olivine. In: Tressler RE and Bradt RC (eds.) *Deformation of Ceramic Materials II. Materials Science Research*, vol. 18, pp. 281–305. New York: Plenum Press.

Pshenichnyuk AI, Astanin VV, and Kaibyshev OA (1998) The model of grain-boundary sliding stimulated by intragranular slip. *Philosophical Magazine* 77: 1093–1106.

Raj R and Ashby MF (1971) On grain boundary sliding and diffusional creep. *Metallurgical Transactions* 2: 1113–1127.

Read WT Jr (1953) *Dislocations in Crystals*, 175pp. New York: McGraw-Hill Book Company.

Read WT and Shockley W (1950) Dislocation models of crystal grain boundaries. *Physical Review* 78: 275–289.

Ready DW (1966) Chemical potentials and initial sintering in pure metals and ionic compounds. *Journal of Applied Physics* 37: 2309–2312.

Ricoult DL and Kohlstedt DL (1983a) Structural width of low-angle grain boundaries in olivine. *Physics and Chemistry of Minerals* 9: 133–138.

Ricoult DL and Kohlstedt DL (1983b) Low-angle grain boundaries in olivine. In: Yan MF and Heuer AH (eds.) *Advances in Ceramics, Character of Grain Boundaries*, vol. 6, pp. 56–72. Columbus: American Ceramic Society.

Ridley N (1995) C.E. Pearson and his observations of superplasticity. In: Ridley N (ed.) *Superplasticity: 60 Years after Pearson*, pp. 1–5. London: Institute of Materials.

Riley GN Jr and Kohlstedt DL (1990) An experimental study of melt migration in an olivine-melt system. In: Ryan MP (ed.) *Magma Transport and Storage*, pp. 77–86. New York: John Wiley & Sons.

Roscoe R (1952) The viscosity of suspensions of rigid spheres. *British Journal of Applied Physics* 3: 267–269.

Ruoff AL (1965) Mass transfer problems in ionic crystals with charge neutrality. *Journal of Applied Physics* 36: 2903–2907.

Rutter EH (1999) On the relationship between the formation of shear zones and the form of the flow law for rocks undergoing dynamic recrystallization. *Tectonophysics* 303: 147–158.

Rutter EH, Brodie KH, and Irving DH (2006) *Journal of Geophysical Research* 111: B06407 (doi:10.1029/2005JB004257).

Rutter EH and Neumann DHK (1995) Experimental deformation of partially molten Westerly granite, with implications for the extraction of granitic magmas. *Journal of Geophysical Research* 100: 15697–15715.

Rybacki E and Dresen G (2000) Dislocation and diffusion creep of synthetic anorthite aggregates. *Journal of Geophysical Research* 105: 26017–26036.

Schmalzried H (1981) *Solid State Reactions,* 2nd edn., 254pp. Weinheim: Verlag Chemie.

Schmalzried H (1995) *Chemical Kinetics of Solids*, 433pp. New York: VCH Publishers.

Schmid S, Boland JN, and Paterson MS (1977) Superplastic flow in fine grained limestone. *Tectonophysics* 43: 257–291.

Scott T and Kohlstedt DL (2006) The effect of large melt fraction on the deformation behavior of peridotite. *Earth and Planetary Science Letters* 246: 177–187.

Sherby OD and Burke PM (1967) Mechanical behavior of crystalline solids at elevated temperature. In: Chalmers B and Hume-Rothery W (eds.) *Progress in Materials Science*. New York: Pergamon Press.

Shewmon PG (1983) *Diffusion in Solids*, 203pp. Jenks, OK: J.Williams Book Company.

Stalder R and Skogby H (2003) Hydrogen diffusion in natural and synthetic orthopyroxene. *Physics and Chemistry of Minerals* 30: 12–19.

Stone DS, Plookphol T, and Cooper RF (2004) Similarity and scaling in creep and load relaxation of single-crystal halite (NaCl). *Journal of Geophysical Research* 109: doi:10.1029/2004JB003064.

Takei Y (2005) Deformation-induced grain boundary wetting and its effects on the acoustic and rheological properties of partially molten rock analogue. *Journal of Geophysical Research* 110: B12203 (doi:10.1029/2005JB003801).

Takei Y and Holtzman BK (2006) Viscous constitutive relations of partially molten rocks in terms of grain-boundary contiguity. *EOS Transactions of the American Geophysical Union* Fall Meeting Supplement 87(52): V23D-0654.

Takeuchi S and Argon AS (1976) Review: Steady-state creep of single-phase crystalline matter at high temperature. *Journal of Material Science* 11: 1542–1566.

Thurel E, Cordier P, Frost D, and Karato S-I (2003) Plastic deformation of wadsleyite. II: High-pressure deformation in shear. *Physics and Chemistry of Minerals* 30: 267–270 (doi: 10.1007/s00269-003-0313-7).

Tsai T-L and Dieckmann R (2002) Variations in the oxygen content and point defects in olivines, $(Fe_x, Mg_{1-x})2SiO_4$, $0.2 \leq x \leq 1.0$. *Physics and Chemistry of Minerals* 29: 680–694.

Tullis J and Yund RA (1980) Hydrolytic weakening of experimentally deformed Westerly granite and Hale albite rock. *Journal of Structural Geology* 2: 439–451.

Tullis J and Yund RA (1985) Dynamic recrystallization of feldspar: A mechanism for ductile shear zone formation. *Geology* 13: 238–241.

von Mises R (1928) Mechanik der plastischen Formänderung von Kristallen. *Zietschrift Angewandten Mathematik und Mechanik* 8: 161–185.

Wanamaker BJ (1994) Point defect diffusivities in San Carlos olivine derived from reequilibration of electrical conductivity following charges in oxygen fugacity. *Geophysical Research Letters* 21: 21–24.

Weertman J (1955) Theory of steady-state creep based on dislocation climb. *Journal of Applied Physics* 26: 1213–1217.

Weertman J (1957a) Steady-state creep through dislocation climb. *Journal of Applied Physics* 28: 362–364.

Weertman J (1957b) Steady-state creep of crystals. *Journal of Applied Physics* 28: 1185–1189.

Weertman J (1978) Creep laws for the mantle of the Earth. *Philosophical Transactions of the Royal Society of London* A 288: 9–26.

Weertman J (1999) Microstructural mechanisms of creep. In: Meyers MA, Armstrong RW, and Kirschner H (eds.) *Mechanics and Materials: Fundamentals and Linkages*, pp. 451–488. New York: Wiley.

Weertman J and Weertman JR (1992) *Elementary Dislocation Theory*, 213pp. Oxford: Oxford University Press.

Xu Y, Nishihara Y, and Karato S-I (2005) Development of a rotational Drickamer apparatus for large-strain high-pressure deformation experiments. In: Chen J, Wang Y, Duffy TS, Shen G, and Dobrzhinetskaya LF (eds.) *Frontier of High-Pressure Research: Applications to Geophysics*, pp. 167–182. Amsterdam: Elsevier.

Xu Y, Weidner DJ, Chen J, Vaughan MT, Wang Y, and Uchida T (2003) Flow-law for ringwoodite in the subduction zone. *Physics of the Earth and Planetary Interiors* 136: 3–9.

Xu Y, Zimmerman ME, and Kohlstedt DL (2004) Deformation behavior of partially molten mantle rocks. In: Karner GD, Driscoll NW, Taylor B, and Kohlstedt DL (eds.) *Rheology and Deformation of the Lithosphere at Continental Margins: MARGINS Theoretical and Experimental Earth Science Series*, vol. 1, pp. 284–310. New York: Columbia University Press.

Zhao Y-H, Ginsberg SG, and Kohlstedt DL (2004) Solubility of hydrogen in olivine: Effects of temperature and Fe content. *Contributions to Mineralogy and Petrology* 147: 155–161 (doi:10.1007/s00410-003-0524-4).

Zimmerman ME and Kohlstedt DL (2004) Rheological properties of partially polten lherzolite. *Journal of Petrology* 45: 275–298.